Nature Communications

https://doi.org/10.1038/s41467-026-68975-3

Article in Press

VSIG10L is a major determinant of esophageal homeostasis and inherited predisposition to Barrett's esophagus

Received: 12 May 2025

Accepted: 9 January 2026

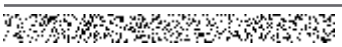

Cite this article as: Ravillah, D., Singh, S., Katabathula, R.M. *et al.* VSIG10L is a major determinant of esophageal homeostasis and inherited predisposition to Barrett's esophagus. *Nat Commun* (2026). https://doi.org/10.1038/s41467-026-68975-3

Durgadevi Ravillah, Salendra Singh, Ramachandra M. Katabathula, Adam M. Kresak, Bhavatharini Udhayakumar, Rajesh Gupta, Wendy Brock, Yosuke Mitani, Vaibhav Jain, Emily Hocke, Simon G. Gregory, Katherine S. Garman, Joel T. Gabre, Hisashi Fujioka, Joseph E. Willis, Amitabh Chak & Kishore Guda

VSIG10L is a Major Determinant of Esophageal Homeostasis and Inherited Predisposition to Barrett's Esophagus

Durgadevi Ravillah[1], Salendra Singh[2], Ramachandra M. Katabathula[1], Adam M. Kresak[3], Bhavatharini Udhayakumar[1], Rajesh Gupta[4], Wendy Brock[4], Yosuke Mitani[5], Vaibhav Jain[6], Emily Hocke[6], Simon G. Gregory[6,7,8], Katherine S. Garman[9], Joel T. Gabre[5], Hisashi Fujioka[10], Joseph E. Willis[3], Amitabh Chak[4,11], Kishore Guda[1,3,4,*]

1. Division of General Medical Sciences–Oncology, Case Comprehensive Cancer Center, Case Western Reserve University School of Medicine, Cleveland, Ohio, USA.
2. Center for Immunotherapy and Precision Immuno-Oncology (CITI), Lerner Research Institute, Cleveland Clinic, Cleveland, Ohio, USA.
3. Department of Pathology, Case Western Reserve University School of Medicine, Cleveland, Ohio, USA.
4. Digestive Health Research Institute, Case Western Reserve University School of Medicine, Cleveland, Ohio, USA.
5. Herbert Irving Comprehensive Cancer Center, Division of Digestive and Liver diseases, Vagelos College of Physicians and Surgeons, Columbia University Irving Medical Center, New York, USA.
6. Duke Molecular Physiology Institute, Duke University School of Medicine, Durham, North Carolina, USA.
7. The Preston Robert Tisch Brain Tumor Center, Duke University School of Medicine, Durham, North Carolina, USA.
8. Department of Neurosurgery, Duke University School of Medicine, Durham, North Carolina, USA.
9. Division of Gastroenterology, Department of Medicine, Duke University, Durham, North Carolina, USA.
10. Cryo-Electron Microscopy Core Facility, Case Western Reserve University School of Medicine, Cleveland, Ohio, USA.
11. Division of Gastroenterology and Hepatology, Case Western Reserve University School of Medicine, Cleveland, Ohio, USA.

***Corresponding Author**

Kishore Guda, DVM., Ph.D., Case Western Reserve University School of Medicine, 2103 Cornell Rd, Cleveland, OH-44106, kkg5@case.edu

ABSTRACT

The molecular underpinnings contributing to the onset of Barrett's esophagus (BE) remain elusive. By studying familial clusters of the disease, here we identify a significant association between genetic variants in the V-set and Immunoglobulin Domain Containing 10 Like (*VSIG10L*) gene and BE predisposition. Using mammalian tissues and patient-derived organoids, we show *VSIG10L* is selectively expressed in the suprabasal squamous cells of the esophageal mucosa and is essential for epithelial maturation and homeostasis. Mice carrying human-orthologous germline mutations in *Vsig10l* exhibit loss of desmosomes, concomitant with disrupted epithelial differentiation programs, in the squamous mucosa. Upon long-term exposure to a bile acid (deoxycholate) supplemented diet, *Vsig10l*-mutant mice develop overt BE-like lesions in the forestomach. Furthermore, loss of esophageal *VSIG10L* expression is observed frequently in patients with chronic gastroesophageal reflux disease, a known risk factor for BE. Collectively, our study uncovers a fundamental link between VSIG10L, esophageal homeostasis, and BE predisposition.

INTRODUCTION

Barrett's esophagus (BE) is characterized by intestinal-type mucinous metaplasia of squamous (SQ) epithelial cells in the distal esophagus [1]. Patients with BE in particular are at a high risk of developing esophageal adenocarcinoma (EAC), an increasingly prevalent and refractory malignancy, often diagnosed at advanced stages where treatments become ineffective [2, 3]. While risk factors for BE/EAC such as age, male gender, Caucasian ethnicity, obesity, gastroesophageal reflux disease (GERD), and diet have been previously suggested, they lack sufficient predictive power to guide effective clinical management of this disease [4, 5, 6]. Moreover, the co-opting genetic / molecular aberrations contributing to the onset and progression of BE remain elusive and complex [7].

Prior studies from our group identified that up to 10% of patients with BE/EAC report a family history, indicating a genetic predisposition to the disease [8, 9, 10, 11, 12]. Our segregation analysis in familial clusters of the disease strongly suggested that familial BE (FBE) is consistent with dominant transmission of one or more incompletely penetrant major Mendelian alleles [13]. Moreover, we have identified genetic linkage of familial BE to distinct chromosomes and genomic loci [8], suggesting that FBE is genetically complex. Using familial association and high-throughput genomic approaches in a large multi-generational index family, we subsequently discovered the first inherited autosomal dominant BE susceptibility variant (S631G) mapped to a highly-conserved Serine residue within the Ig-like domain in the V-set And Immunoglobulin Domain Containing 10 Like (*VSIG10L*) gene[14].

Here we sought to determine the extent of *VSIG10L* susceptibility variants in a large cohort of BE/EAC familial kindreds. Furthermore, we characterized the expression of *VSIG10L* in esophageal mucosa, developed human-orthologous *Vsig10l*-mutant mice, and performed

molecular and phenotypic studies to interrogate the pathogenicity of *VSIG10L* variants. Overall, our study identifies VSIG10L as a key molecule involved in maintaining esophageal homeostasis; defects in which enhance susceptibility to BE.

RESULTS

Identification of familial BE/EAC-associated susceptibility variants in *VSIG10L*

In follow-up to our previous report [14], here we determined the extent of *VSIG10L* susceptibility variants associated with the disease by targeted sequencing of *VSIG10L* coding regions in 684 blood DNA samples, banked from BE/EAC affected and unaffected relatives from 302 families, accrued through an active multi-center familial BE registry [8, 14, 15]. We found additional rare/private germline *VSIG10L* susceptibility variants including: a rare deleterious frameshift deletion (dbSNP: rs1185522503, Minor Allele Frequency[16]: 0.0001) in a 50 year old female diagnosed with BE; a private missense variant (GRCh37/hg19/chr19:51842243: A>A/G, p.V543A) in a male diagnosed with BE at age 61; and a rare in-frame deletion (dbSNP: rs370588522, Minor allele frequency[16]: 0.0027) in a male diagnosed with EAC at age 82. Together, our studies in familial clusters of the disease indicated a pathogenetic link between VSIG10L and BE/EAC predisposition.

VSIG10L expression is localized to suprabasal squamous cells of the esophagus

VSIG10L is predominantly expressed in SQ cells, and its gene product encodes a membrane-bound protein with immunoglobulin (Ig)-like domains [14]. Nonetheless, its function in the esophagus or in other SQ tissues is hitherto unknown. We accordingly first sought to determine its expression within the stratified esophageal SQ mucosa. Given the lack of optimized VSIG10L antibodies, we developed custom RNAscope-*in situ* hybridization probes and subsequently assessed its expression in representative human and porcine esophagus, as well as in human SQ

epithelial cells (EPC2) grown as 3D-organotypes [17, 18]. As shown in Figure 1, we found *VSIG10L* RNA to be selectively and consistently expressed in suprabasal SQ cells, with no detectable expression in basal squamous cells, suggesting a possible role of VSIG10L in epithelial maturation.

Esophageal organoids from *VSIG10L*-mutant patient show disrupted squamous maturation. We previously reported that EPC2 3D-organotypes engineered to express the *VSIG10L*-S631G FBE variant exhibit dysmaturation and loss of epithelial integrity, while ultrastructural assessments of esophageal mucosa from the *VSIG10L* S631G-mutant patient revealed loss of desmosomes and dilated intercellular spaces particularly within the suprabasal SQ cells [14]. To further explore the impact of VSIG10L on the developmental dynamics of esophageal SQ cells, we generated and assessed esophageal progenitor SQ organoids derived from pluripotent stem cells (hPSC) from the *VSIG10L*-S631G patient. Morphologically, organoids from the *VSIG10L*-S631G patient showed frequent disruption of SQ epithelial stratification and maturation, in stark contrast to the normal(anticipated) growth and differentiation of SQ organoids observed in the control subject grown under the same experimental conditions. Immunohistochemistry (IHC) assessments revealed that the single layer of cells in the abnormal glandular-appearing organoids in the mutant patient to be positive for p63 (basal SQ cell marker), albeit to varying degree, suggesting these may be predominantly basal-like SQ cells (Fig. 2). Additionally, unlike in the control subject, the spherical-appearing organoids from the mutant patient often showed loss of inward epithelial differentiation gradient, with strong p63-positivity in all the cells (Fig. 2), further suggesting a perturbation in SQ maturation. Together, these findings point to VSIG10L as an essential component involved in maintaining normal SQ maturation and architecture.

Mice mutant for *Vsig10l* exhibit ultrastructural and molecular abnormalities in the squamous forestomach

Given our above and prior [14] observations implying a potential role of VSIG10L in sustaining SQ homeostasis, we next sought to interrogate the pathogenicity of familial BE-associated *VSIG10L* variants, *in vivo*. Accordingly, we generated the following human-orthologous germline *Vsig10l*-mutant murine models on a C57Bl/6J background: 1) Based on the human FBE variant (*VSIG10L*-S631G [14]), we generated mice carrying the orthologous *Vsig10l*-S516G missense mutation, mapping to the highly conserved Serine residue within the Ig-like domain [14]; and 2) Based on the deleterious frameshift variant (rs1185522503) identified in one of our familial BE kindreds mentioned above, we additionally generated mice that were null / knockout (KO) for *Vsig10l*.

First, similar to our observations in human and porcine tissues (Fig. 1), we found murine *Vsig10l* to be also selectively expressed in the subprabasal cells of the SQ mucosa (Fig. 3a). As BE typically develops in the distal portion of the esophagus contiguous with the gastro-esophageal (SQ-columnar) junction [1], we next assessed for potential ultrastructural changes within the SQ mucosa of the forestomach in the *Vsig10l*-mutant mice, using Transmission Electron Microscopy (TEM). Both S516G and KO mice revealed a marked reduction in desmosomes in the suprabasal SQ cell layer where *VSIG10L* is expressed (Fig. 3b). Importantly, our findings in the *Vsig10l*-mutant mice are remarkably consistent with the ultrastructural changes we observed in the esophagus of familial BE patient carrying the orthologous germline *VSIG10L* S631G variant [14], suggesting a potential role of VSIG10L in maintaining epithelial integrity that is conserved across species. To further understand the molecular programs impacted by *Vsig10l* disruption, we performed Spatial Transcriptomic Profiling (STP) using formalin-fixed and paraffin–embedded (FFPE) tissues derived from the SQ forestomach of representative wild type and *Vsig10l*-mutant

mice (Fig. 3c). Subsequent gene set enrichment analysis of STP profiles revealed a significant disruption of cell structure and differentiation programs in the SQ mucosa of both S516G and KO mice (Fig. 3c). To orthogonally evaluate our TEM and STP findings, we assessed the expression of Desmogleins (Dsg1/3), members of the cadherin gene family and key components of desmosomes involved in cell-cell adhesion and epidermal cell differentiation [19, 20], in an independent set of wild type and *Vsig10l*-mutant mice. Immunohistochemistry (IHC) analyses of FFPE SQ tissues indeed showed a reduction of Dsg1 protein in S516G-mutant mice, with a more pronounced repression of both Dsg1 and Dsg3 proteins in the KO mice, compared to the wild type (Fig. 3d). Collectively, these findings add further support to the role of VSIG10L in maintaining SQ epithelial integrity and maturation.

Of note, in analyzing the STP data, we explored whether *Vsig10l* disruption additionally leads to perturbations in downstream effectors / signaling pathways, using our in-house developed computational framework, InFlo [18, 21, 22]. While no significant changes in canonical signaling pathways or large signaling networks were observed, few individual sub-networks showed altered activities in the *Vsig10l*-mutant mice compared to wild type (Supplementary Figure 1). While some of these differentially-activated components such as Notch, Bmp, Smad have been implicated in BE/EAC pathobiology [23], characterizing their functional relationship with VSIG10L (direct or indirect) and the broader significance of such changes in these specific nodes / components require further in-depth investigations.

Vsig10l-mutant mice develop BE-like mucinous metaplasia lesions upon chronic exposure to reflux-associated injury

Since factors disrupting epithelial homeostasis can render the esophagus more susceptible to GERD injury and BE pathogenesis [7, 24, 25], we posited *Vsig10l*-mutant mice may exhibit an inherent

propensity to developing BE-like pathologies upon exposure to deoxycholate (DCA), a key bile acid involved in reflux injury and a risk factor for BE [26, 27, 28, 29]. Accordingly, wild type and *Vsig10l*-mutant mice were fed either standard diet or diet supplemented with 0.2% DCA, and followed longitudinally for a period of up to 24 months. Mice were then sacrificed, and esophageal, forestomach contiguous with the SQ-columnar junction, and gastric tissues were harvested. Respective FFPE tissue sections were subsequently subjected to histopathological examination. Tissues were primarily assessed for the presence of BE-like lesions, hereafter referred to as Barrett's-like mucinous metaplasia (BEMM), by a gastrointestinal pathologist (J.E.W) who was blinded to the sample genotypes. Subsequently, the incidences of BEMM lesions in mice were enumerated across respective heterozygous and homozygous *Vsig10l* genotypes. While no noticeable pathologies were observed in the standard diet group, the vast majority (70%-100%) of *Vsig10l*-mutant mice on DCA diet developed BEMM lesions at the SQ-columnar junction in the forestomach, significantly different from the infrequent diminutive lesions developing in ~20% of wild type mice (Fig. 4). Importantly, BEMM lesions developing in *Vsig10l*-mutant mice were also qualitatively quite distinct than those developing in wild type; i.e, BEMM lesions in the *Vsig10l*-mutant mice were more exacerbated and extensive, unlike the occasional and minor / restricted glandular changes observed in the wild type mice (Fig. 5). Beyond histomorphometric similarities, BEMM lesions in *Vsig10l*-mutant mice exhibited molecular features that are characteristic of human BE, including: induction of intestinal-type acidic mucins [30, 31, 32]; expression of BE-associated mucin, Mucin 6 (Muc6) [33, 34, 35]; induction of Trefoil Factor 3 (Tff3), a BE-associated trefoil protein and a marker of established intestinal columnar metaplasia and true goblet cells [36, 37]; as well as SRY-Box Transcription Factor 9 (Sox9), a key transcription factor implicated in BE pathogenesis that drives columnar differentiation of esophageal SQ epithelium [38] (Fig. 5). Also,

similar to human BE, BEMM lesions in these mice were negative for the SQ marker, p63 (Fig. 5). We further note that no such abnormal lesions or gross histologic changes were apparent elsewhere in the esophagus proper in the *Vsig10l*-mutant mice. Collectively, these findings underscore the pathogenicity of FBE-associated *VSIG10L* susceptibility variants in facilitating BE development.

Esophageal SQ mucosa from GERD patients reveal a loss of *VSIG10L* expression

As injury from chronic reflux is a key risk factor for the onset of BE [4, 5, 6], we further sought to conversely determine whether GERD-associated injury to esophageal SQ mucosa can impact *VSIG10L* expression. Accordingly, we accrued a random set of snap-frozen distal esophageal SQ tissue biopsies from non-familial patients with GERD, and subsequently assessed *VSIG10L* RNA expression using real-time qPCR. Of note, erosive or ulcerative esophagitis cases were excluded from this analysis. Compared to a random cohort of non-GERD subjects, esophageal tissues from GERD patients showed a significantly lower *VSIG10L* expression (~3-fold, $P = 0.008$), while no such differences were observed in *TP63* (SQ marker) RNA between the two cohorts (Fig. 6a). To further orthogonally assess *VSIG10L* expression in the context of GERD, we performed RNAscope-*in situ* hybridization in distal esophageal FFPE tissue sections, derived from an independent set of five GERD patients and two control subjects that were available for testing. In stark contrast to healthy / normal SQ epithelia, we found a profound reduction of *VSIG10L* expression or a near-all depletion of *VSIG10L*-positive differentiation gradient in the stratified SQ layer of GERD-associated reactive esophageal mucosa (Fig. 6b). As anticipated, we observed an expansion of basal-like immature SQ cells expressing p63 particularly in these reactive mucosal regions from GERD patients (Fig. 6b). Taken together, these findings provocatively suggest that GERD-associated disruption of *VSIG10L* dynamics in the esophageal mucosa may be one of the

early molecular changes by which reflux injury impairs SQ homeostasis and potentially enhances the risk of further BE development.

DISCUSSION

The cellular origins of BE are likely multifaceted, with several sources including esophageal SQ cells being suggested as potential BE progenitors [39, 40]. In line with this, prior genome-wide association and our familial studies have identified a pathogenetic correlation between genes involved in maintaining esophageal SQ integrity / maturation and risk of BE/EAC development [14, 41, 42]. Our prior [14] and current studies on VSIG10L in human tissues, relevant *ex vivo* / *in vitro* models, and *Vsig10l*-mutant mice now provide strong evidence underscoring its essential role in maintaining SQ maturation and integrity, and *per se*, point to the likely pathogenic role of FBE-associated *VSIG10L* genetic variants. Further, our observation of BE-like pathologies occurring only in the presence of DCA in the *Vsig10l*-mutant mice suggest that disruption in SQ homeostasis caused by these mutations produce a risky field, and over time, in the presence of chronic GERD injury with concomitant reflux of bile acids, promote BE pathogenesis. Alternatively, inherited or acquired defects in *VSIG10L* may impair normal healing of reflux-associated injury to SQ mucosa in at-risk individuals, consequently facilitating BE predisposition. Taken together, our findings suggest a plausible hypothesis where a perturbation in SQ homeostasis, much like that observed in GERD, may be one of the key initial processes in the development of BE. In this regard, inherited defects in *VSIG10L* could disrupt epithelial homeostasis, and render the SQ mucosa more prone to reflux injury and/or abnormal healing following injury, thus enhancing risk of BE development (Fig. 7). In the absence of such inherent predisposition, homeostasis is often restored due to normal healing of the injured esophagus; however, in certain instances, GERD-induced

injury to SQ mucosa, concomitant with acquired VSIG10L disruption and additional genetic / epigenetic alterations, could potentially hinder normal healing and promote BE development (Fig. 7).

In regard to Barrett's esophagus and related neoplasia, we would also like to emphasize that existing *in vitro* / *ex vivo* experimental models have significant conceptual and technical limitations that preclude mimicking the pathogenesis of a complex disorder like BE. Furthermore, unlike other common gastrointestinal cancers, there are certain limitations to consider when utilizing surrogate animal models for studying BE/EAC. First, contrary to humans, esophageal mucosa in mice are keratinized, lack submucosal glands, and the stratified SQ epithelium extends from esophagus into mouse forestomach [43, 44, 45]. These anatomical distinctions may pose challenges in fully capturing the complexity of human gastroesophageal (patho)biology in mice. In fact, the small number of murine BE models available to date do not robustly mimic human disease, and furthermore were not based on genetic defects pertinent to BE pathogenesis and predisposition in humans [43, 44, 45]. Second, it remains unclear why BEMM lesions occur exclusively at the SQ-columnar junction and not elsewhere in the esophagus. Our findings are also in line with the *IL1β*-mediated inflammatory murine model where pathologic changes were restricted to the SQ-columnar junction [46]. It is likely that the SQ-columnar (gastro-esophageal) junction may remain the primary site for reflux injury allowing the backflow of stomach acid resulting in metaplastic changes when compared to the esophagus, or that cellular heterogeneity in esophagus may underlie differential response to reflux injury along the length of esophagus compared to SQ-columnar junction. Prior studies have also proposed transitional cells at the SQ-columnar junction as a potential source of BE progenitors [47]. It is possible that these cells at the SQ-columnar transitional zone are inherently more plastic to intrinsic or extrinsic stresses, and future studies are indeed

warranted to elucidate these lines of investigations. Third, while our familial studies show association of germline *VSIG10L* variants with risk of BE as well as EAC development [14], we did not observe any cancers in the *Vsig10l*-mutant mice. This lack of a cancer phenotype is consistent with available animal models in this disease context [43, 44, 45]. It is possible that longer follow-up studies, additional genetic, epigenetic, mutagen, and/or dietary changes need to be considered to facilitate the development of cancer in mice. Also, VSIG10L remains largely uncharacterized, and our prior [14] and current translational investigations were predominantly geared towards identifying *VSIG10L* susceptibility variants and determining their pathogenicity and biologic consequences, a critically-important step in ascertaining causality. Further comprehensive studies are indeed needed to fully decipher the biochemical and regulatory aspects of VSIG10L.

The discovery of pathogenic variants in genes such as *APC* and *BRCA1/2* from studies of rare families have led to key insights into the molecular pathogenesis of colorectal and breast cancers. Similarly, our discovery of genes involved in BE/EAC predisposition [14, 48], such as *VSIG10L*, from studies of FBE families should provide critical molecular insights into metaplasia-dysplasia-cancer progression, identify targets for developing chemopreventive / therapeutic drugs, and enable development of genetic tests for early screening for BE/EAC susceptibility. Moreover, the human-orthologous *Vsig10l*-mutant murine models we developed here should provide a more relevant physiologic system to study disease pathogenesis as well as for interrogating potential dietary and/or chemical modulators associated with BE development, progression, and/or prevention.

METHODS

Our research study complies with relevant ethical regulations. Written informed consent was obtained from all donors for use of their samples and clinical data in the present study. All human

protocols were approved by University Hospitals Cleveland Medical Center Institutional Review Board (IRB) for human investigations (CASE 3207 CC301) and Duke GI Tissue Repository (protocol number; 00001662), adherent to the principles outlined in the Declaration of Helsinki. PBMC-derived human pluripotent stem cells from the *VSIG10L* S631G mutant patient and control subject were obtained under an IRB-approved protocol (CASE 3207 CC301) with written consent, and included MTA agreements where appropriate. Archived Porcine tissues were accessed through North Carolina State University (NCSU), approved by NCSU Institutional Animal Care and Use Committee-approved protocol (NCSU 13-116-B). All mouse studies were approved by Case Western Reserve University Institutional Animal care and Use Committee (IACUC), and conform to the ARRIVE 2.0 [49] guidelines. A flow diagram illustrating all the experiments performed and reported in the current study is provided in Supplementary Figure 2.

Familial patients and VSIG10L DNA sequencing

Probands with BE or EAC as well as unaffected controls were recruited and gave written informed consent for collection of biopsy tissues and blood for research as part of the Barrett's Esophagus Translational Network (BETRNet) Consortium using a consent and biobanking protocol (protocol number, CASE 3207 CC30) approved by the Institutional Review Board for Human Investigation at University Hospitals Cleveland Medical Center and collaborating institutions [8, 12, 13, 14, 15], adherent to the principles outlined in the Declaration of Helsinki. The observational study is registered at clinicaltrials.gov, NCT00288119. Study subjects were given a questionnaire that collects information about BE and EAC risk factors along with family history. Study subjects provide written consent to use banked biospecimens for genetic studies and other future research. Permission is also obtained from probands to contact their relatives. Histologic diagnosis for family members reported to have BE or EAC is confirmed by review of records whenever

available. Family members who had no prior esophagogastroduodenoscopy (EGD) were offered screening. Blood or saliva is banked from probands and family members who are alive and consent to the study. Study subjects gave written consent and blood lymphocytes were collected, immortalized, and banked at the Rutgers University DNA Repository (RUCDR) as a source of germline DNA from all family members who had screening endoscopy. For deceased family members, permission is obtained from nearest living relatives to obtain formalin fixed paraffin embedded (FFPE) biopsy tissues from treating hospitals. Germline DNA was extracted from blood, immortalized lymphocytes, saliva, or FFPE tissues for subsequent sequencing. Targeted capture and DNA resequencing of *VSIG10L* exons in 684 samples, belonging to 302 families, was performed by Novogene (Sacramento, CA). Of the 684 subjects, 428 were men and 256 women (self-reported), mean age was 61.5 years (range; 14-100 yrs), and all familial BE subjects were of European ancestry. Only samples passing internal quality controls were included in the analysis. Raw 100-bp FASTQ reads were aligned to the human reference genome (hg19) using the Burrows-Wheeler Aligner (BWA-v0.7.17) [50]. Alignment quality was assessed with GATK Picard tools (v2.18.12), followed by pre-processing of BAM files with a custom script utilizing GATK [51] to mark duplicates, recalibrate base quality scores, and realign indels. For variant calling, we used two independent callers; UnifiedGenotyper [52] and HaplotypeCaller [53] from the GATK Suite. Variant calls were filtered to exclude those with coverage below 30 reads or an alternate base frequency under 0.1. Filtered variants were annotated using Oncotator (v1.9.1.0) [54], and were further analyzed for population-level allele frequencies using the ExAC [55] and gnomAD (v4.1.0) [56] databases. All rare/private variants were further manually reviewed using Integrative Genomics Viewer [57]. Lastly, selected variants were orthogonally confirmed in fresh DNA aliquots from respective samples using direct Sanger sequencing.

Porcine tissue procurement

Archival porcine esophageal tissue blocks of normal squamous epithelium were accessed for the *VSIG10L* localization assays. All porcine tissues were originally derived from Yorkshire crossbred pigs (Sus scrofa) of either sex, weighing approximately 35 kg, and cared for according to North Carolina State University Institutional Animal Care and Use Committee-approved protocol (NCSU 13-116-B) and as set forth in the Guide for the Care and Use of Laboratory Animals, published by the National Institutes of Health. Porcine tissues were collected by North Carolina State University Large Animal Models Core of the Center for Gastrointestinal Biology and Disease (CGIBD) under veterinary supervision [58]. For euthanasia, initial sedation was provided with xylazine-ketamine injection, and then animals were euthanized with pentobarbital (60mg/kg IV) and clinically assessed by veterinary staff to confirm death prior to collection of esophageal tissues that were subsequently used for histologic analyses.

Generation of Vsig10l mutant mice

Vsig10l S516G missense mutant (orthologous to the human *VSIG10L* variant S631G [14]) and *Vsig10l* knockout (KO) (targeted deletion of Exon 1- Exon 10) mice were generated on a C57Bl/6J (The Jackson Laboratory, Bar Harbor, ME) genetic background (Strain no:000664), using standard CRISPR-Cas9 methodology. Briefly, single guide RNAs (sgRNAs) for generating murine *Vsig10l* (Gene ID: 75690) S516G and KO were selected using the CRISPR design tool (http://crispr.mit.edu/) [59]. In the end, the following sgRNA sequences (5'-3') were selected for the missense S516G mutant (CGACTACAGCTTAGCCAGGA on exon 6), and for the KO (upstream-ACCTGGGACAATGCAAGCTG; downstream-AGGACTGGACCCTAAGAGTG). Cleavage efficiency of the selected sgRNAs were confirmed using the Guide-it Complete sgRNA Screening System (TakaraBio USA Inc, San Jose, CA; cat. no. 632636), with C57Bl/6J mouse genomic DNA

as the template. PAGE-purified sgRNAs along with Cas9 protein (PNA Bio, CA) were microinjected into fertilized eggs and implanted into pseudopregnant females to generate mice with precise genomic edits at specific loci. For the S516G mutant, the following PAGE-purified donor ultramer was co-injected: 5'-CTCGGCAAGGACGGCCCCTGGCTCCAGGTGGTGGGGGCCGACTACAGCTTGGCCAAGATGGCCGAAAGCTCCTCATCAACAACTTCAGCCTGGATTGGGA. Tail DNA extracted from the pups were confirmed for genomic editing using the Illumina Miseq platform (San Diego, CA) for founder mice. F1 founder mice were selected following confirmation of germline transmission by backcrossing with wild type C57Bl/6J mice. The above CRISPR-based *Vsig10l* mutant mice were generated in collaboration with the Transgenic and Targeting facility at Case Western Reserve University (CWRU). All animal studies were approved by Case Western Reserve University Institutional Animal care and Use Committee (IACUC), under the protocol number 2019-0082, and were handled in compliance with the 3Rs (Replacement, Reduction and Refinement) ethics guidelines. All wild type and *Vsig10l* mutant mice were housed in the CWRU animal core facility and maintained on a standard 12h:12h light-dark cycle, 70-74°F temperature, and ~50% humidity. The *Vsig10l*-mutant mouse models developed here will be shared with other investigators upon request and following review by the corresponding author to ensure that distribution complies with ethical, institutional, and material-transfer guidelines.

Breeding and genotyping of Vsig10l mutant mice

Homozygous *Vsig10l* mutant mice (S516G and KO) were viable and exhibited fair breeding performances. Genotyping was performed using DNA isolated from tail digests. Briefly, mutant mice for S516G were genotyped using PCR-Sanger sequencing with primer sequences on Exon 6 (forward; TGCTGCTCCAGCCCATAGT, reverse; TGGACCTGAGAGAGGGTGATT,

amplicon size of 361bp). *Vsig10l* KO mice were genotyped using conventional PCR amplification with primer sequences upstream of Exon 1 (forward; TGGGCTTCTCCATACAACCTC) and downstream of Exon 10 (reverse; TGCCAACCACATTCATCCGT) resulting in an amplicon size of 401bp for the deleted region. Genotypes of heterozygous mice (-/+) were confirmed using the above primers as well as PCR amplification of the wild type Exon 9 region (forward; GCTCACCCCACCAGCAAAAA, reverse; ACAGTGGGAGGCAACGACAC), resulting in 401bp and 139bp products. PCR conditions included initial denaturation at 95˚C for 4min, followed by 40 cycles of 95˚C for 30 sec, 66˚C (S516G) or 58˚C (KO) annealing for 45 sec, and 72˚C extension for 45 sec. All animal procedures were approved by CWRU in accordance with Institutional Animal care and Use Committee (IACUC) and followed the National Institutes of Health guidelines.

Animal diet and tissue harvest

Animals were fed either standard irradiated diet containing 12 kcal% fat with Palm Oil (Research Diet Inc, NJ; cat. no. 19102101), or standard irradiated diet containing 12 kcal% fat with Palm Oil supplemented with 0.2% Deoxycholic Acid (Millipore Sigma-Aldrich, cat no. D2510; Research Diet Inc; cat. no. 19102102) starting at 5 weeks of age and for a period of 24 months. Animals within each genotype were randomly assigned to the respective standard or standard plus DCA diet groups. The diets were stored in cold dry place. Mice were allowed to have ad libitum access to respective diets (replenished weekly), and drinking water was supplied through standard sipper tubes during the entire duration of the study. At the end of the study, esophagus and forestomach from each mouse were isolated, formalin-fixed (10% neutral buffer) and paraffin–embedded (FFPE) for subsequent histopathologic and molecular assessments. The overall sex distribution of the mice available for final analyses (N=46) were 50% male and 50% female; wild type (50%

male), *Vsig10l* S516G/+ (58% male), *Vsig10l* S516G/S516G (44% male), *Vsig10l -/+* (57% male), *Vsig10l -/-* (38% male). As genetic predisposition can enhance BE/EAC risk in both men and women [8, 15, 60], data from both male and female mice in respective genotypes were pooled for all analysis. All animal experiments were conducted in accordance with the ARRIVE 2.0 guidelines [49].

EPC2 squamous 3D-Organotypic culture model

EPC2 human esophageal squamous esophageal cell line (EPC2), originally derived from a male non-BE patient [14, 18, 61], was gifted to us by Dr. John P. Lynch MD, Ph.D at University of Pennsylvania. Briefly, EPC2 cells were grown in serum free keratinocyte-SFM media (Thermo Fisher scientific, Waltham, MA; cat no. 17005042), supplemented with Bovine Pituitary Extract (BPE, Thermo Fisher scientific; cat no. 13028-014) and human recombinant epidermal growth factor (rEGF, Thermo Fisher scientific; cat no. 10450-013), and maintained at 37°C and 5% CO_2. Cells were tested for authenticity using short tandem repeat genotyping and were screened periodically for mycoplasma contamination. EPC2 3D-organotypes were generated as follows: Transwell inserts were added to deep-well six-well plates. 3D collagen/Matrigel matrices (bottom and top layer in the transwell insert) were prepared on Day1. The bottom layer was prepared using 10X EMEM (BioWhittaker, Walkersville, MD; cat no. 12-684F), Fetal Bovine serum (Hyclone, Logan, UT; cat no. SH30088.3), L-glutamine (Cellgro, Corning, NY; cat no. 25-005-CI), sodium bicarbonate (BioWhittaker; cat no. 17-613E) and high concentration (2.2mg/ml) collagen rat tail (Corning; cat no. 354249). The reagents were mixed well and incubated at 37˚C for 20 minutes to let the matrix solidify. The top layer of the insert was prepared by mixing 10X EMEM, FBS, L-glutamine, Sodium bicarbonate, collagen, matrigel (Corning; cat no. 354234), and 7.5 X 10^4 human esophageal fibroblasts (ScienCell, Carlsbad, CA; cat. no. 2730), and then added to the

bottom of the transwell. On Day7, media was changed to Dulbecco's Modified Eagles Medium (Sigma-Aldrich, St. Louis, MO; cat no. 51441C) and Ham's F-12 (Gibco, Grand Island, NY; cat no. 11765-054) in a 3:1 ratio and added to the bottom and top of the transwell and incubated for 1hr at 37˚C. Media was then removed from the top and approximately 1.5 X 10^6 EPC2 cells were added as droplets. After a 2-hour incubation at 37˚C, Epidermalization I media was added to the plate supplemented with the following: DMEM, F-12, L-glutamine, Hydrocortisone (Sigma-Aldrich, cat no. H0888), ITES (500x) (Biowhittaker; cat no. 17839Z), O-phoshory-ethanolamine (Sigma-Aldrich; cat no. P0503), adenine (Sigma-Aldrich; cat no. A9795), progesterone (Sigma-Aldrich; cat no. P8783), triiodothyronine (Sigma-Aldrich; cat no. T5516), newborn calf serum chelated (Hyclone; cat no. SH3011802). On Day 11, media was removed and the Epidermalization II medium was added to the bottom of the plate only, allowing the epithelial cells to differentiate at the air-liquid interface. Epidermalization I and II media have similar components, except that no progesterone is added to Epidermalization II media. On day 17 organotype cultures were harvested by fixing in 10% formaldehyde (Thermo Fisher Scientific; cat.no. SF100-4), and later were paraffin-embedded for further histopathological analysis.

RNAscope In Situ Hybridization

RANscope ISH was performed on 5 μM FFPE sections [62] derived from human, porcine and mouse tissues, using the RNAscope 2.5 HD Single-plex Chromogenic Assay kit as per the manufacturer's instructions (Advanced Cell Diagnostics, Newark, CA; Cat no. 322360). Briefly, 5 μM tissue / organoid sections were baked for 60 mins at 60˚C, de-paraffinized in xylene for 5 minutes twice and rehydrated in 100% ethanol for 3 minutes and air dried for 5 minutes. The sections were then quenched with hydrogen peroxide for 10 minutes at room temperature and heat-induced RNA Scope antigen retrieval was carried out at 100-104˚C for 15 minutes. Following antigen-retrieval,

slides were rinsed quickly in distilled water at room temperature and dipped in 100% ethanol for 2 minutes and air dried for 5 minutes. The sections were covered with RNA Scope protease plus, followed by incubation in a humidity-controlled oven for 25 min at 40˚C and rinsed in distilled water. Sections were then subjected to *VSIG10L* ISH with custom RNAscope-ISH probes, designed using Advanced Cell Diagnostics RNAscope probe design pipeline, against respective human (cat. no. 1086661-C1), pig (cat. no. 1161521-C1) or mouse (cat. no. 1088591-C1) species. ISH probe hybridization was carried out in a humidity-controlled oven for 120 minutes at 40˚C. Following hybridization, sections were washed in RNA scope 1X wash buffer atleast twice for 2 minutes at room temperature. Sections were subsequently processed for signal amplification using RNA scope amplification reagent 1 in a humidity-controlled oven for 30 minutes at 40˚C. Following amplification, sections were rinsed with RNA scope 1X wash buffer atleast twice for 2 minutes at room temperature. The above step was repeated with amplification reagents 2, 3, and 4, followed by rinsing with RNA Scope 1X wash buffer for each section. Sections were then incubated with amplification reagent 5 and 6 for 15- 30 minutes at room temperature with intermittent rinsing using RNA scope 1X wash buffer atleast twice for 2 minutes at room temperature. Sections were then covered with Fast Red Chromagen (Advanced Cell Diagnostics; cat. no. 322360) by using a 60:1 dilution of Buffer Fast Red A: Chromagen Fast Red B for 3-5minutes. After decanting the chromagen, 120µl of 3,3'-Diaminobenzidine chromogen (DAB) mixture was added to each section and incubated at room temperature for 10 minutes. Sections were then rinsed in distilled water and stained with CAT Hematoxylin counter stain (Biocare Medical, Pacheco, CA; cat. no. CATHE-M) for 30 seconds, rinsed under running tap water for 30 seconds, followed by additional rinses in distilled water for 1 minute atleast three times. Cell nuclei were stained with bluing reagent for one minute with TBST wash buffer and rinsed in running tap

water for 30 seconds and dehydrated in Xylene, and cover slipped with Ecomount medium (Biocare Medical; cat. no. EM897L). Tissue/organoid sections were also stained for standard Hematoxylin and eosin (H&E) for histologic characterization in respective serial sections. Stained sections were visualized using EVOS M7000 imaging system (Thermo Fisher Scientific). All images were captured using identical settings on the EVOS M7000 imaging system, and each tissue section on a slide was imaged in its entirety using the M7000 image tile-stitching software function.

Electron microscopy

Esophageal tissues from euthanized mice were prepared for electron microscopy using the protocol previously described by us [14, 63, 64]. Briefly, tissues were fixed with triple aldehyde-DMSO fixative for 2h at room temperature. The specimens were thoroughly rinsed in 0.1 M phosphate buffer, pH 7.4, then post-fixed for 2h in an unbuffered 1:1 mixture of 2% osmium tetroxide and 3% potassium ferricyanide. After rinsing with distilled water, the specimens were soaked overnight in an acidified solution of 0.25% uranyl acetate. After another rinse in distilled water, they were dehydrated in ascending concentrations of ethanol, passed through propylene oxide, and embedded in Poly/Bed resin mixture. Thin sections were sequentially stained with acidified uranyl acetate followed by a modification of Sato's triple lead stain and examined in a FEI Tecnai Spirit (T12) transmission electron microscope with a 4k x 4k Gatan US4000 CCD camera.

Spatial Transcriptomics

The Visium Spatial Gene Expression platform from 10x Genomics was used for spatial transcriptomic profiling (STP). Briefly, esophageal FFPE tissue sections (5 μM) from wild type and *Vsig10l* mutant mice (with DV200 ≥ 80%) were placed within a 6.5mm^2 field on a 10x Genomics gene expression slide that contains 5,000 barcoded probes. Sections were deparaffinized

via xylene immersion, ethanol to remove the solubilized paraffin, and then immersion in water to remove residual ethanol. The deparaffinized tissues were then stained with hematoxylin and eosin (H&E) to visualize tissue architecture. RNA sequestered by formalin fixation within the tissue is de-crosslinked by serial treatment with HCl at room temperature followed by heating at 70˚C in TE buffer pH 9.0 for 1 h. Next, cells within the tissue were permeabilized prior to RNA hybridization with whole transcriptome mouse probe panels (21k), consisting of RNA-templated ligation (RTL) probes that target the protein-coding transcriptome. Following targeted gene probe ligation, the poly-A tail from probes were then used as template for the on-surface probe priming. Probes were extended by the addition of a UMI, Spatial Barcode and partial Read 1, then released from the slide and collected for qPCR to optimize sample index PCR cycle number. Targeted gene products then underwent index PCR to ligate Illumina sequencing adapters and sample dual indices followed by final library cleanup by SPRI select size selection. Final libraries were assessed on a Tapestation 4200 and quantified by qPCR. Libraries were sequenced on Illumina NGS paired end sequencers at 25k reads/spot on an Illumina paired end, dual indexed flowcell in the format of 28x10x10x50. Data were then uploaded to analyses packages for visualization.

Gene Set Enrichment analyses (GSEA)

Spatial transcriptomics gene expression data from wild type and *Vsig10l* mutant mice were subjected to Gene Set Enrichment analyses (GSEA) using the fgsea package in R. This analyses aimed to pinpoint pathways and biological processes significantly enriched among the differentially expressed genes (DEGs) between the experimental groups: Wild type vs. S516G; Wild type vs. KO. Gene sets were sourced from multiple databases, including the Molecular Signatures Database (MSigDB), Gene Ontology (GO), KEGG, and Reactome, encompassing curated pathways and gene ontologies. The input for GSEA consisted of ranked gene lists based

on log2 fold change values for differential expression between the aforementioned comparisons. For each analyses, GSEA calculated an enrichment score (ES) for each gene set, indicating the extent to which the genes within that set were overrepresented at the top or bottom of the ranked gene list. The significance of the ES was determined through permutation testing (1,000 permutations), which yielded a normalized enrichment score (NES). We considered gene sets with a false discovery rate (FDR) q-value of <0.05 to be significantly enriched.

Immunohistochemistry

Immunohistochemical evaluation was performed using standard protocols and methods as previously described by our group [18, 22]. Briefly, 5 μM mouse and human tissue / organoid sections were baked for 75 minutes at 60˚C followed by de-paraffinization in xylene and subsequent rehydration in series of graded ethanols (100%, 95%, 70% respectively) and rinsed in distilled water. Heat-induced antigen retrieval was carried out in a pressure cooker in citrate solution (pH 6.0) at 123˚C for 30 seconds and endogenous peroxidase was quenched with 3% hydrogen peroxide for 8 minutes. Charged proteins and endogenous IgG was blocked in background sniper solution for 20 minutes. Slides were incubated with the primary Dsg1 (Abcam; cat. no. ab124798, 1:1000 dilution), Dsg3 (Thermo Fisher; cat. no. BS-6585R, 1:400 dilution), Muc6 (Thermo Fisher; cat. no. PA5-79706, 1:1500 dilution), Tff3 (Thermo Fisher; cat. no. 14-4758-82, 1:5000 dilution), Sox9 (Abcam; cat. no. ab185230, 1:1000 dilution), p63 (GeneTex, cat. no. GTX102425, 1:100 dilution), or CK7 (Abcam, cat. no. ab181598, 1:50,000) overnight at 4˚C. Detection of antibodies was achieved by incubating the tissue sections with anti-mouse or anti-rabbit horseradish peroxidase (HRP) conjugated polymers for 30 minutes. Sections were stained with 3,3'-Diaminobenzidine chromogen for 5 minutes to visualize the antigen-antibody binding, and hematoxylin was used as a nuclear counterstain. Stained sections were visualized using the EVOS

M7000 imaging system (Thermo Fisher Scientific). In parallel, FFPE sections were subjected to standard Alcian blue/Periodic Acid Schiff's stain procedure to evaluate the presence of mucins. Briefly, 5 μM esophageal and forestomach tissue sections were deparaffinized and hydrated with distilled water. Sections were then placed in Alcian Blue (AB) pH 2.5 stain solution for 30 minutes at room temperature, and rinsed with deionized water. Subsequently, sections were placed in Periodic acid solution (PAS) for 5 minutes at room temperature, rinsed with deionized water, followed by staining with Schiff's reagent for 15 minutes and rinsed with deionized water. All sections were counter stained with hematoxylin 7211 for one minute, rinsed, and followed by staining with bluing reagent for one minute. Sections were dehydrated in anhydrous alcohol followed by clearing and mounting. The acidic mucosubstances appear blue in color and the neutral polysaccharides appear purple/magenta in color. All images were captured using identical settings on the EVOS M7000 imaging system, and each tissue section on a slide was imaged in its entirety using the M7000 image tile-stitching software function. As appropriate, IHC findings were assessed on a qualitative scale for the presence or absence of signal (yes or no) in a blinded fashion.

Human PSC-derived esophageal organoids

PBMC-derived human pluripotent stem cells (hPSC) were generated from the *VSIG10L* S631G mutant patient who had provided written consent under the protocol approved by the Institutional Review Board for Human Investigation at the University Hospitals Cleveland Medical Center [14]**.** The control BU3 hPSC line [65], derived from a healthy male Caucasian, was purchased from Boston university stem cell core under an MTA agreement and approved informed consent. Esophageal progenitor cells (EPCs) were subsequently derived from the hPSCs as previously described [66]. Briefly, hPSCs were first cultured in mTeSR plus medium (Stemcell technologies, Vancouver, BC; cat. no. 85850) on 6-well plates coated with 100x diluted Matrigel. After 24 hours, the medium

was replaced with Definitive Endoderm Medium plus supplements MR and CJ (StemCell Technologies; cat. no. 05110). After additional 24 hours of culture (day 2), the media was replaced and cells incubated in Definitive Endoderm (DE) medium plus supplement CJ. At day 3, the media was replaced again with fresh DE media plus supplement CJ. At day 4, Serum-Free Differentiation (SFD) Media was prepared as following: 375 ml of reconstituted Iscove's DMEM (Corning, Corning, NY; cat. no. 15-016-CV), 125 ml of Ham's F-12 (Corning; cat. no.10-080-CV), 5 ml of N2 (Thermo Fisher Scientific; cat. no. 17502048), 10 ml of B27 (Thermo Fisher Scientific; cat. no. 12587010), 3.3 ml of 7.5% Bovine Albumin Fraction V Solution (Thermo Fisher Scientific; cat. no. 15260037), 19.6 µl of 11.5 M monothioglycerol (Sigma-Aldrich, St. Louis, MO; cat. no. M6145), 500 µl of L-Ascorbic acid (Sigma-Aldrich; cat. no. A92902) and 1 ml of 50 mg/ml primocin (Invitrogen, Waltham, MA; cat. no. NC9141851). At day 4, the cells were passaged into new Matrigel-coated 6-well plates as clusters and cells were further induced by culturing in the SFD medium plus 10 µM SB431542 (Selleckchem, Houston, TX; cat. no. S1067), 200 ng/ml Noggin (R&D Systems, Minneapolis, MN; cat. no. 6057-NG),100 ng/ml EGF (Peprotech, Cranbury, NJ; cat. no. AF-100-15) and 10µM Y-2763210 (Selleckchem; cat. no. S1049) for 24 hours and the SFD medium plus 10 µM SB431542, 200 ng/ml Noggin and 100 ng/ml EGF for another 48 hours (day 5-6). Cells were maintained at 5% O2/ 90% N2/ 5% CO2 from day 1-6. To induce esophageal progenitor cell differentiation, anterior cells were cultured from day 7 to day 16 in the SFD medium plus 10 µM SB431542, 200 ng/ml Noggin and 100 ng/ml EGF. From day 16 to day 24, cells were maintained in the SFD medium plus 100 ng/ml EGF. Cells were cultured at 95% air/ 5% CO2 from day 7 onwards. On day 24, the cells were sorted using FACS to obtain EPCs. To perform cell surface marker staining, cells were disassociated with Accutase added DNase (Thermo Fisher Scientific) and 10 µM Y-2763210 and stained with PE/Cyanine7 anti-

human CD326 (EpCAM) antibody (BioLegend, San Diego, CA; cat. no. 324201) in FACS buffer (1× PBS, 2% FBS, added DNase and 10 μM Y-2763210) for 1 hour with live/dead staining dye SYTOX (Thermo Fisher Scientific; cat. no. S7020) to exclude dead cells. Stained cells were analyzed using BD FACS CariaII (BD Biosciences, Franklin Lakes, NJ) and sorted EPCAM-positive cells. Sorted hPSCc-derived EPCs were counted and seeded at 20,000 cells per 50 μL Geltrex (Thermo fisher Scientific; cat. no. A1413202) per one well of a 24-well plate, and the medium was added to after Geltrex solidified. The organoid culture medium included the SFD medium, supplemented with 10 μM Y27632, 10 μM SB431542, 10 μM GSK3 inhibitor (Stem cell technologies; cat. no. CHIR99021), 20 ng/ml FGF2 and 200 ng/ml EGF. hPSC-derived EPC 3D-organoids were subsequently FFPE embedded, sectioned, and used for analysis.

Semi-quantitative PCR analysis of VSIG10L in GERD vs. non-GERD biopsy tissues

Endoscopically-normal appearing mucosal biopsies were collected from the distal 5 cm of the squamous esophagus from control patients without BE or EAC during upper endoscopy who consented under the observational study biobanking protocol approved by the Institutional Review Board for Human Investigation of the University Hospitals Cleveland Medical Center [9]. Esophageal samples from Duke University hospitals were obtained from participants who enrolled in the GI Tissue Repository, and longitudinal observational study of patients presenting for endoscopic procedures who agreed to use of excess clinical samples approved by the Institutional Review Board for Human Investigation at Duke Universtiy Medical Center (protocol number; 00001662), adherent to the principles outlined in the Declaration of Helsinki. Archival samples from research participants were accessed through CWRU and Duke BioRepository & Precision Pathology Center (BRPC). Clinical data were collected and updated, including demographics, gastrointestinal symptoms, endoscopic and pathologic findings as previously described [67]. Chronic

GERD was defined as the presence of at least weekly heartburn or regurgitation for at least five years as assessed by the Mayo gastroesophageal reflux questionnaire (GERQ) [68]. Erosive or ulcerative esophagitis cases were not included. Non-GERD was defined as either none or less than once a month heartburn or regurgitation for less than five years. All biopsy tissues were snap-frozen at the site of collection. Among the GERD subjects (n=23), 77% were men and 23% were women (self-reported), and the mean age of the sampled cohort at the time of diagnosis was 54.7 years (range; 28-77 yrs). 92% of GERD subjects were of European ancestry and 8% Asians. All but 4 of the subjects with GERD were on proton pump inhibitors or histamine-2 blockers. For the non-GERD control cohort (n=24), 73% were men and 27% were women (self-reported), and the mean age of the sampled cohort was 60.1 years (range; 41-80 yrs). 96% of non-GERD control subjects were of European ancestry and 4% African Americans. Total RNA was extracted from respective distal esophageal squamous biopsies using RNeasy Plus Mini kit (Qiagen, Germantown, MD; cat. no. 74134,). Subsequently, 0.5-1 μg of total RNA was reverse-transcribed using Superscript IV First-Strand Synthesis (Thermo Fisher Scientific; cat. no. 18091) according to the manufacturer's protocol. qPCR of *VSIG10L* (Qiagen; cat. no. QT02451393), *TP63* (Qiagen; cat. no. QT02424051), and beta-2-microglobulin (*B2M)* (Qiagen; cat. no. QT00088935) were performed using iQ SYBR Green Supermix (Bio-Rad Laboratories, Hercules, CA; cat. no. 170-8887) on the CFX96 system (Bio-Rad). *TP63* was used as a control for SQ epithelial content in the biopsy tissues and *B2M* was used as an endogenous control for RNA. Each qPCR reaction was carried out in triplicates and the mean expression levels across the triplicates were normalized to the mean expression values of *B2M* using the ΔCt method. A two-tailed non-parametric Mann-Whitney U test was used to determine significant differences in expression between GERD vs non-GERD tissues.

Statistics & Reproducibility

Data analyses and pertinent statistical tests are outlined in respective Methods sub-sections above. Sample size estimations or randomization were not applicable for human genetic studies, as all individuals that were accrued were sequenced. The study focuses on identifying BE susceptibility variants in *VSIG10L* in affected families. Unaffected/healthy family relatives were sequenced where available. To assess the minor allele frequencies of the detected *VSIG10L* variants in families, large-scale population databases like gnomAD and ExAC were used. Results from gene expression studies in human samples were estimated using non-parametric tests. For animal studies, assuming 80% power and a significance level of 0.05, 6 mice in each group will enable detecting ≥50% metaplasia incidence (qualitative estimates) with a 95% CI of±28.1. For diet studies, respective age-matched genotype mice were randomly assigned to the standard or DCA diet groups, and dietary interventions were initiated at the same age across genotypes. *Vsig10l*-mutant genotypes were compared to respective wild type littermates in all instances. Results from animal expression studies were also estimated using non-parametric tests, and additional multiple testing corrections were performed for STP datasets where appropriate. Where appropriate, biologic/technical replicates were included in the experiments to confirm reproducibility of the results. As stated before, mouse genotypes were blinded for all subsequent histopathologic and electron microscopy assessments. No data were excluded for either human or animal studies.

DATA AVAILABILITY

All data supporting the findings of this study are available within the manuscript. Respective publicly-accessible databases (such as gnomAD and ExAC) were cited within the main text. Sharing of *VSIG10L* raw DNA sequencing data from familial subjects will be considered following formal written request by investigators to the corresponding author. All requests pertaining to the

data in the current study will be processed in 3-5 weeks from the date of request. All data access requests will undergo in-depth review by University Hospitals Cleveland Medical Center Institutional Review Board (and by a genetic counselor) to ensure that distribution complies with ethical, institutional, and material-transfer guidelines, while ensuring strict confidentiality of the familial relationships. Source data are provided with this paper.

REFERENCES

1. Stawinski PM, Dziadkowiec KN, Kuo LA, Echavarria J, Saligram S. Barrett's Esophagus: An Updated Review. *Diagnostics (Basel)* **13**, (2023).

2. Siegel RL, Kratzer TB, Giaquinto AN, Sung H, Jemal A. Cancer statistics, 2025. *CA Cancer J Clin* **75**, 10-45 (2025).

3. Rubenstein JH, Shaheen NJ. Epidemiology, Diagnosis, and Management of Esophageal Adenocarcinoma. *Gastroenterology* **149**, 302-317 e301 (2015).

4. Shaheen NJ, Falk GW, Iyer PG, Gerson LB, American College of G. ACG Clinical Guideline: Diagnosis and Management of Barrett's Esophagus. *Am J Gastroenterol* **111**, 30-50; quiz 51 (2016).

5. American Gastroenterological A, Spechler SJ, Sharma P, Souza RF, Inadomi JM, Shaheen NJ. American Gastroenterological Association medical position statement on the management of Barrett's esophagus. *Gastroenterology* **140**, 1084-1091 (2011).

6. Spechler SJ. Clinical practice. Barrett's Esophagus. *The New England journal of medicine* **346**, 836-842 (2002).

7. Que J, Garman KS, Souza RF, Spechler SJ. Pathogenesis and Cells of Origin of Barrett's Esophagus. *Gastroenterology* **157**, 349-364 e341 (2019).

8. Chak A, *et al.* Familial aggregation of Barrett's oesophagus, oesophageal adenocarcinoma, and oesophagogastric junctional adenocarcinoma in Caucasian adults. *Gut* **51**, 323-328 (2002).

9. Chak A, *et al.* Identification of Barrett's esophagus in relatives by endoscopic screening. *Am J Gastroenterol* **99**, 2107-2114 (2004).

10. Juhasz A, Mittal SK, Lee TH, Deng C, Chak A, Lynch HT. Prevalence of Barrett esophagus in first-degree relatives of patients with esophageal adenocarcinoma. *J Clin Gastroenterol* **45**, 867-871 (2011).

11. Sun X, *et al.* Linkage and related analyses of Barrett's esophagus and its associated adenocarcinomas. *Mol Genet Genomic Med* **4**, 407-419 (2016).

12. Sun X, *et al.* Predicting Barrett's Esophagus in Families: An Esophagus Translational Research Network (BETRNet) Model Fitting Clinical Data to a Familial Paradigm. *Cancer Epidemiol Biomarkers Prev* **25**, 727-735 (2016).

13. Sun X, *et al.* A segregation analysis of Barrett's esophagus and associated adenocarcinomas. *Cancer Epidemiol Biomarkers Prev* **19**, 666-674 (2010).

14. Fecteau RE, *et al.* Association Between Germline Mutation in VSIG10L and Familial Barrett Neoplasia. *JAMA Oncol* **2**, 1333-1339 (2016).

15. Chak A, *et al.* Familiality in Barrett's esophagus, adenocarcinoma of the esophagus, and adenocarcinoma of the gastroesophageal junction. *Cancer Epidemiol Biomarkers Prev* **15**, 1668-1673 (2006).

16. Karczewski KJ, *et al.* The mutational constraint spectrum quantified from variation in 141,456 humans. *Nature* **581**, 434-443 (2020).

17. Harada H, *et al.* Telomerase induces immortalization of human esophageal keratinocytes without p16INK4a inactivation. *Mol Cancer Res* **1**, 729-738 (2003).

18. Venkitachalam S, *et al.* The Ephrin B2 Receptor Tyrosine Kinase Is a Regulator of Proto-oncogene MYC and Molecular Programs Central to Barrett's Neoplasia. *Gastroenterology* **163**, 1228-1241 (2022).

19. Kowalczyk AP, Green KJ. Structure, function, and regulation of desmosomes. *Prog Mol Biol Transl Sci* **116**, 95-118 (2013).

20. Green KJ, Simpson CL. Desmosomes: new perspectives on a classic. *J Invest Dermatol* **127**, 2499-2515 (2007).

21. Dimitrova N, *et al.* InFlo: a novel systems biology framework identifies cAMP-CREB1 axis as a key modulator of platinum resistance in ovarian cancer. *Oncogene* **36**, 2472-2482 (2017).

22. Blum AE, *et al.* Systems Biology Analyses Show Hyperactivation of Transforming Growth Factor-beta and JNK Signaling Pathways in Esophageal Cancer. *Gastroenterology* **156**, 1761-1774 (2019).

23. Maslenkina K, *et al.* Signaling Pathways in the Pathogenesis of Barrett's Esophagus and Esophageal Adenocarcinoma. *Int J Mol Sci* **24**, (2023).

24. Fitzgerald RC. Molecular basis of Barrett's oesophagus and oesophageal adenocarcinoma. *Gut* **55**, 1810-1820 (2006).

25. Tobey NA, Carson JL, Alkiek RA, Orlando RC. Dilated intercellular spaces: a morphological feature of acid reflux--damaged human esophageal epithelium. *Gastroenterology* **111**, 1200-1205 (1996).

26. Souza RF. From Reflux Esophagitis to Esophageal Adenocarcinoma. *Dig Dis* **34**, 483-490 (2016).

27. Masaoka T, Suzuki H. Does Bile Reflux Influence the Progression of Barrett's Esophagus to Adenocarcinoma? (Gastroenterology 2013;145:1300-1311). *J Neurogastroenterol Motil* **20**, 124-126 (2014).

28. Quante M, Abrams JA, Lee Y, Wang TC. Barrett esophagus: what a mouse model can teach us about human disease. *Cell Cycle* **11**, 4328-4338 (2012).

29. Prichard DO, *et al.* Deoxycholic acid promotes development of gastroesophageal reflux disease and Barrett's oesophagus by modulating integrin-alphav trafficking. *J Cell Mol Med* **21**, 3612-3625 (2017).

30. Morales TG, Sampliner RE. Barrett's esophagus: update on screening, surveillance, and treatment. *Arch Intern Med* **159**, 1411-1416 (1999).

31. Chen YY, *et al.* Significance of acid-mucin-positive nongoblet columnar cells in the distal esophagus and gastroesophageal junction. *Hum Pathol* **30**, 1488-1495 (1999).

32. Goldblum JR. Barrett's esophagus and Barrett's-related dysplasia. *Mod Pathol* **16**, 316-324 (2003).

33. Niv Y, Fass R. The role of mucin in GERD and its complications. *Nat Rev Gastroenterol Hepatol* **9**, 55-59 (2011).

34. Arul GS, Moorghen M, Myerscough N, Alderson DA, Spicer RD, Corfield AP. Mucin gene expression in Barrett's oesophagus: an in situ hybridisation and immunohistochemical study. *Gut* **47**, 753-761 (2000).

35. Warson C, *et al.* Barrett's esophagus is characterized by expression of gastric-type mucins (MUC5AC, MUC6) and TFF peptides (TFF1 and TFF2), but the risk of carcinoma

development may be indicated by the intestinal-type mucin, MUC2. *Hum Pathol* **33**, 660-668 (2002).

36. Paterson AL, Gehrung M, Fitzgerald RC, O'Donovan M. Role of TFF3 as an adjunct in the diagnosis of Barrett's esophagus using a minimally invasive esophageal sampling device-The Cytosponge(TM). *Diagn Cytopathol* **48**, 253-264 (2020).

37. Dunn LJ, Jankowski JA, Griffin SM. Trefoil Factor Expression in a Human Model of the Early Stages of Barrett's Esophagus. *Dig Dis Sci* **60**, 1187-1194 (2015).

38. Clemons NJ, *et al.* Sox9 drives columnar differentiation of esophageal squamous epithelium: a possible role in the pathogenesis of Barrett's esophagus. *Am J Physiol Gastrointest Liver Physiol* **303**, G1335-1346 (2012).

39. Garman KS. Origin of Barrett's Epithelium: Esophageal Submucosal Glands. *Cell Mol Gastroenterol Hepatol* **4**, 153-156 (2017).

40. Rhee H, Wang DH. Cellular Origins of Barrett's Esophagus: the Search Continues. *Curr Gastroenterol Rep* **20**, 51 (2018).

41. Palles C, *et al.* Polymorphisms near TBX5 and GDF7 are associated with increased risk for Barrett's esophagus. *Gastroenterology* **148**, 367-378 (2015).

42. Levine DM, *et al.* A genome-wide association study identifies new susceptibility loci for esophageal adenocarcinoma and Barrett's esophagus. *Nature genetics* **45**, 1487-1493 (2013).

43. Martinez-Uribe O, Becker TC, Garman KS. Promises and Limitations of Current Models for Understanding Barrett's Esophagus and Esophageal Adenocarcinoma. *Cell Mol Gastroenterol Hepatol* **17**, 1025-1038 (2024).

44. Kapoor H, Lohani KR, Lee TH, Agrawal DK, Mittal SK. Animal Models of Barrett's Esophagus and Esophageal Adenocarcinoma-Past, Present, and Future. *Clin Transl Sci* **8**, 841-847 (2015).

45. Macke RA, *et al.* Barrett's esophagus and animal models. *Ann N Y Acad Sci* **1232**, 392-400 (2011).

46. Quante M, *et al.* Bile acid and inflammation activate gastric cardia stem cells in a mouse model of Barrett-like metaplasia. *Cancer Cell* **21**, 36-51 (2012).

47. Jiang M, *et al.* Transitional basal cells at the squamous-columnar junction generate Barrett's oesophagus. *Nature* **550**, 529-533 (2017).

48. Garman KS, *et al.* Caveolin-3 Null Mutation in Family with Barretts Esophagus and Esophageal Adenocarcinoma. *bioRxiv*, (2021).

49. Percie du Sert N, *et al.* The ARRIVE guidelines 2.0: Updated guidelines for reporting animal research. *PLoS Biol* **18**, e3000410 (2020).

50. Li H, Durbin R. Fast and accurate short read alignment with Burrows-Wheeler transform. *Bioinformatics* **25**, 1754-1760 (2009).

51. McKenna A, *et al.* The Genome Analysis Toolkit: a MapReduce framework for analyzing next-generation DNA sequencing data. *Genome Res* **20**, 1297-1303 (2010).

52. DePristo MA, *et al.* A framework for variation discovery and genotyping using next-generation DNA sequencing data. *Nature genetics* **43**, 491-498 (2011).

53. Poplin R, *et al.* Scaling accurate genetic variant discovery to tens of thousands of samples. *bioRxiv*, 201178 (2018).

54. Ramos AH, *et al.* Oncotator: cancer variant annotation tool. *Hum Mutat* **36**, E2423-2429 (2015).

55. Karczewski KJ, *et al.* The ExAC browser: displaying reference data information from over 60 000 exomes. *Nucleic Acids Res* **45**, D840-D845 (2017).

56. Gudmundsson S, *et al.* Variant interpretation using population databases: Lessons from gnomAD. *Hum Mutat* **43**, 1012-1030 (2022).

57. Robinson JT, *et al.* Integrative genomics viewer. *Nat Biotechnol* **29**, 24-26 (2011).

58. Kruger L, *et al.* Ductular and proliferative response of esophageal submucosal glands in a porcine model of esophageal injury and repair. *Am J Physiol Gastrointest Liver Physiol* **313**, G180-G191 (2017).

59. Hsu PD, *et al.* DNA targeting specificity of RNA-guided Cas9 nucleases. *Nat Biotechnol* **31**, 827-832 (2013).

60. Drovdlic CM, *et al.* Demographic and phenotypic features of 70 families segregating Barrett's oesophagus and oesophageal adenocarcinoma. *J Med Genet* **40**, 651-656 (2003).

61. Kalabis J, *et al.* Isolation and characterization of mouse and human esophageal epithelial cells in 3D organotypic culture. *Nat Protoc* **7**, 235-246 (2012).

62. Ravillah D, *et al.* Discovery and Initial Characterization of Long Intergenic Noncoding RNAs Associated With Esophageal Adenocarcinoma. *Gastroenterology* **165**, 505-508 e507 (2023).

63. Fujioka H, Tandler B, Cohen M, Koontz D, Hoppel CL. Multiple mitochondrial alterations in a case of myopathy. *Ultrastruct Pathol* **38**, 204-210 (2014).

64. Fujioka H, *et al.* Multiple muscle cell alterations in a case of encephalomyopathy. *Ultrastruct Pathol* **38**, 13-25 (2014).

65. Jacob A, *et al.* Differentiation of Human Pluripotent Stem Cells into Functional Lung Alveolar Epithelial Cells. *Cell Stem Cell* **21**, 472-488 e410 (2017).

66. Zhang Y, *et al.* 3D Modeling of Esophageal Development using Human PSC-Derived Basal Progenitors Reveals a Critical Role for Notch Signaling. *Cell Stem Cell* **23**, 516-529 e515 (2018).

67. Abbas G, Pennathur A, Keeley SB, Landreneau RJ, Luketich JD. Laser ablation therapies for Barrett's esophagus. *Semin Thorac Cardiovasc Surg* **17**, 313-319 (2005).

68. Locke GR, Talley NJ, Weaver AL, Zinsmeister AR. A new questionnaire for gastroesophageal reflux disease. *Mayo Clin Proc* **69**, 539-547 (1994).

ACKNOWLEDGMENTS

This research was supported by Public Health Service (PHS) awards: P01 CA269019 (A.C., K.S.G., S.G.G., J.E.W., K.G.); Case GI SPORE P50 CA150964 (K.G.), P30 CA043703 (K.G.); R01 DK118022 (K.S.G.); P30 DK034987 (K.S.G.); P30 CA014236 (S.G.G.); P30 DK097948 (A.C.); U01 CA271867 (A.C., J.E.W.); The DeGregorio Family Foundation (K.G.), Torrey Coast Foundation GEMINI Network (K.G.), and The Gastric Cancer Foundation (K.G.). This work was also supported by the Animal Resource Center, Transgenic and Targeting core, Tissue Resources Core at the Case Western Reserve University, Molecular Genomics Core at Duke University, and Duke's BioRepository & Precision Pathology Center (BRPC).

We are grateful to the patients who opt to participate in our research. We thank our co-author, late Dr. Fujioka, who passed away recently, for his expert advice and help with electron microscopy studies that served as the foundation for understanding the biology of VSIG10L. We thank late Dr. Nathan A. Berger at Case Western Reserve University, who passed away recently, for expert scientific guidance and advice during the conceptualization phase of this study. We thank late Ms. Anne Baskin at Case Western Reserve University who also passed away recently for her technical assistance in animal husbandry. We thank Ms. Lakshmeswari Ravi for her technical input on the experimental methodologies used in this study. We thank the clinical gastroenterology providers who collect research samples from enrolled participants under their clinical care, especially Dr. Rahul Shimpi and Dr. Michael Feiler, as well as the Gastroenterology Clinical Research Unit staff at Duke. We thank Thomas C. Becker for performing lab-based assays in the Garman Lab to support this project.

AUTHOR CONTRIBUTIONS

Study concept and design (D.R., A.C., K.G.); Acquisition of data (D.R., A.M.K., B.U., R.G., W.B., Y.M., V.J., E.H., K.S.G., S.G.G., J.T.G., H.K., A.C., K.G.); Analysis and interpretation of data (D.R., S.S., R.M.K., V.J., S.G.G., J.T.G., H.K., J.E.W., A.C., K.G.); Drafting of the manuscript (D.R.); Critical revision of the manuscript (A.C., K.G.); Statistical analysis (R.M.K.); Obtained funding (A.C., K.G.); Administrative, technical, or material support (W.B., R.G., A.C., K.G.); Study supervision (K.G.).

COMPETING INTERESTS

The authors declare no competing interests

FIGURE LEGENDS

Figure 1: Localization of *VSIG10L* in esophageal squamous mucosa. (Top row) H&E staining of representative human and porcine esophagus FFPE tissue sections, as well as normal esophageal squamous cell line EPC2 grown in 3-dimensional organotypic culture (3D-OTC), showing stratified esophageal squamous mucosa. Images are oriented with luminal side towards the top and basal squamous layer at the bottom. **(Bottom row)** Custom RNAscope-*in situ* hybridization (ISH) analyses of respective tissue sections revealing *VSIG10L* RNA selectively expressed and localized in suprabasal squamous epithelial cell layers (magenta dots), and absent in basal squamous cells. Magnified insets of regions (rectangular boxes) are shown within each of the respective panels, as necessary. All *VSIG10L* ISH analyses were optimized *a priori*, and were tested on four human and porcine biologic replicate tissue sections to ascertain reproducibility. Scale bar, 200μM.

Figure 2: Impaired SQ maturation and architecture of esophageal organoids derived from *VSIG10L*-mutant patient. Shown are serial sections of H&E staining and p63 (SQ marker) IHC of hPSC-derived esophageal SQ organoids from *VSIG10L*(S631G)-mutant BE patient, and a control subject. Respective magnified insets provided on the right show representative areas of the organoids. Note the disrupted morphology and SQ stratification of the organoids from *VSIG10L*(S631G)-mutant patient, compared to the anticipated normal architecture and stratification of esophageal SQ organoids observed in the control subject. Cells in the abnormal glandular-appearing organoids (blue arrows) in the mutant patient show variable nuclear p63 reactivity. Furthermore, note the lack of epithelial differentiation gradient with a near-all p63-positivity in the majority of spherical/solid organoids (red arrows) from the mutant patient; compared to the normal differentiation pattern of the spherical/solid organoids in the control subject (i.e. strong p63-positivity in the basal cells in the circumference and the gradual loss of

p63-reactivity in the differentiated cells towards the center). H&E staining and p63 IHC were performed on duplicate organoid serial sections to ensure reproducibility. Scale bar, 250µM.

Figure 3: Perturbation of structural and differentiation programs in the SQ forestomach of *Vsig10l*-mutant mice. **(a)** H&E staining of squamous mucosa in 24-month old wild type and *Vsig10l*-mutant (S516G, KO) mice. Images are oriented with luminal side towards the top and sub-mucosal layer at the bottom. Scale bar, 200µM. RNAscope-ISH of murine *Vsig10l* in corresponding serial sections revealing its selective localization in suprabasal cells (magenta dots), while absent in basal squamous cells. As anticipated, *Vsig10l* expression was absent in KO mice. *Vsig10l* ISH was performed in three mice per genotype to ensure reproducibility. **(b)** Transmission electron microscopy (TEM) analyses of squamous mucosa in wild type and *Vsig10l*-mutant mice. Note the marked reduction in desmosomes (yellow arrows, magnified view) in *Vsig10l*-mutant compared to wild-type mice. TEM assessments were performed in duplicates per genotype to ensure reproducibility. Scale bar (pink), 2µM. **(c)** Shown at the top-left is H&E image and corresponding Spatial Transcriptomics Profiling (STP) cluster plot depicting distinct clusters in squamous forestomach, gastric mucosa, and squamo-columnar junction in a wild type mouse. Scale bar, 200µM. Shown to the right is the t-SNE projection, along with a few exemplar genes representing the different cell types. For example, Cluster 2 is derived from SQ forestomach cells, whereas Cluster 4 from gastric cells. Shown to the right are UMAP plots demonstrating normalized *Vsig10l* expression across genotypes. Shown at the bottom is STP-based gene set enrichment analyses (GSEA) of differentially expressed genes (DEG) revealing a significant suppression of structural and differentiation programs in squamous mucosa of *Vsig10l*-mutant mice, compared to wild type. CC (cellular component); BP (Biologic process); MF (Molecular function). Gene sets with a false discovery rate (FDR) q-value of <0.05 were considered statistically significant. Source

data are provided as a Source Data file. STP profiling was performed in duplicate tissue sections to ensure reproducibility. **(d)** IHC analyses of murine Desmogleins 1 and 3 (Dsg1,3) in SQ tissues, showing decreased Dsg1 protein levels in *Vsig10l*-mutant mice, with further pronounced loss of Dsg1&3 in KO mice, compared to wild type. Dsg1,3 IHC was performed in duplicate tissue sections to ensure reproducibility. Scale bar, 150µM.

Figure 4: Augmentation of Barrett's-like Mucinous Metaplasia (BEMM) at the SQ-columnar junction in *Vsig10l*-mutant mice. FFPE tissue sections from 24-month old wild type, S516G, and KO mice on DCA diet were subjected to histopathological examination, where genotypes were blinded to the pathologist. The x-axis of the bar graph shows the different genotypes, including both heterozygous and homozygous for the S516G and KO mice, along with the number of mice in parenthesis available for histopathologic assessment. Y-axes represents the incidence percent of normal vs. BEMM phenotype (at the SQ-columnar junction) in respective genotypes. The provided P-values were estimated using a one-tailed Fisher's Exact test, comparing wild type vs. respective *Vsig10l*-mutant genotypes. (#) indicates significant differences between wild type and indicated genotypes at $P = 0.0125$ following further Bonferroni multiple hypothesis testing correction. Source data are provided as a Source Data file.

Figure 5: BEMM lesions in *Vsig10l*-mutant mice recapitulate the histologic and molecular characteristics of human BE. Histologic assessments of SQ-columnar junction from two representative mice (m1, m2), per respective genotypes, are shown. Green arrows indicate SQ-columnar junction. Note the BEMM lesions in *Vsig10l*-mutant mice are more pronounced, replacing a large portion of SQ-columnar junction and adjacent gastric mucosa, unlike the diminutive and restricted changes observed in wild type mice. Respective BE and SQ markers were assessed using IHC and AB-PAS (Alcian blue/Periodic Acid Schiff's). BEMM glandular

lesions containing abundant intestinal-type acidic mucins show intense blue staining, whereas neutral mucins associated with gastric foveolar epithelium stain magenta (AB-PAS). Also note the intense staining of Muc6 (dense cytoplasmic brown staining), Tff3 (dark brown intracellular staining with round to oval appearance), and Sox9 (nuclear staining), along with absence of p63 (squamous epithelial marker) within the BEMM lesions in *Vsig10l*-mutant mice. Histopathologic assessments were performed in all mice available for testing (from Figure 4) per respective genotype in a blinded fashion. Subsequent IHC analyses were performed in four mice (biologic replicates) per respective genotype to ensure reproducibility. Scale bar, 250μM.

Figure 6: Chronic reflux injury suppresses *VSIG10L* expression in the distal esophagus. (a) Real time qPCR analyses of *VSIG10L* and *TP63* RNA in distal esophageal squamous (SQ) biopsy tissues from patients without or with GERD. qPCR was performed in triplicate reactions per sample per gene, and *B2M* expression was used as an endogenous house-keeping control. Y-axes indicate fold-change (FC) in *VSIG10L* and *TP63* expression in GERD and non-GERD samples, normalized to the average expression of the respective genes in the non-GERD samples. Each black dot overlaid on the bar graphs represents normalized qPCR value of individual sample. Error bars indicate mean ± s.d. Significant differences in expression levels between GERD vs. non-GERD were estimated using two-tailed non-parametric Mann-Whitney U test. Note the ~3-fold lower *VSIG10L* expression in GERD compared to non-GERD tissues. *TP63*, used as a control for squamous epithelial content in the biopsy tissues, showed no significant difference (*n.s*) between the two cohorts. Source data are provided as a Source Data file**. (b)** Distal esophageal FFPE tissue sections from two non-GERD subjects and five GERD patients (P1-P5) were subjected to H&E, *VSIG10L* ISH, and p63 IHC analyses. Control and GERD subjects were >18 yrs old, male (self-reported), and were of European ancestry, with the exception of GERD - P3 patient who was an

African American Female (self-reported). GERD patients were on proton pump inhibitors or histamine-2 blockers. All images were oriented with luminal side towards the top and basal SQ cell layer at the bottom. Note the strong *VSIG10L* expression (magenta dots) in the subprabasal SQ cells in normal / healthy tissues from non-GERD control subjects. In contrast, note the marked reduction or depletion of *VSIG10L*-positive differentiated cells, concomitant with an expansion of basal-like p63-positive immature cells (brown nuclear staining), in GERD-associated reactive SQ mucosa. ISH and IHC assessments were performed on duplicate tissues sections from all control subjects and GERD patients to ensure technical reproducibility. Scale bar, 200µM.

Figure 7: A hypothetical representation on the potential role of VSIG10L in BE pathobiology. Chronic injury such as GERD can lead to disruption of SQ mucosa, proliferation of basal-like immature SQ cells, and inflammation; in a normal state, repair and healing of such injured epithelium regenerates esophageal SQ mucosa and restores homeostasis. However, inherited or acquired defects in VSIG10L can lead to impaired SQ homeostasis, and in conjunction with GERD, could compromise restoration of injured epithelia, and likely facilitate abnormal metaplastic healing and BE predisposition. Of note, it remains unclear (?) whether GERD induces hyperplasia of basal-like immature SQ cells which subsequently leads to loss of VSIG10L-positive differentiated cells, or whether GERD suppresses VSIG10L expression which then disrupts SQ maturation leading to expansion of basal-like SQ cells. Also, the above assumptions are based on the likely role of VSIG10L in maintaining SQ architecture and maturation, and there could be additional (yet to be determined) regulatory and functional aspects of VSIG10L that are involved in BE pathogenesis. Further comprehensive studies are warranted to ascertain these presumptions and to fully dissect the function of VSIG10L.

Editorial Summary

The factors contributing to the onset of Barrett's esophagus, a precancerous stage of the highly lethal esophageal cancer, remain elusive. Here, the authors identify inherited mutations in the VSIG10L gene as a key etiologic determinant affecting esophageal biology and facilitating the development of Barrett's esophagus.

Peer review information: *Nature Communications* thanks the anonymous, reviewers for their contribution to the peer review of this work. A peer review file is available.

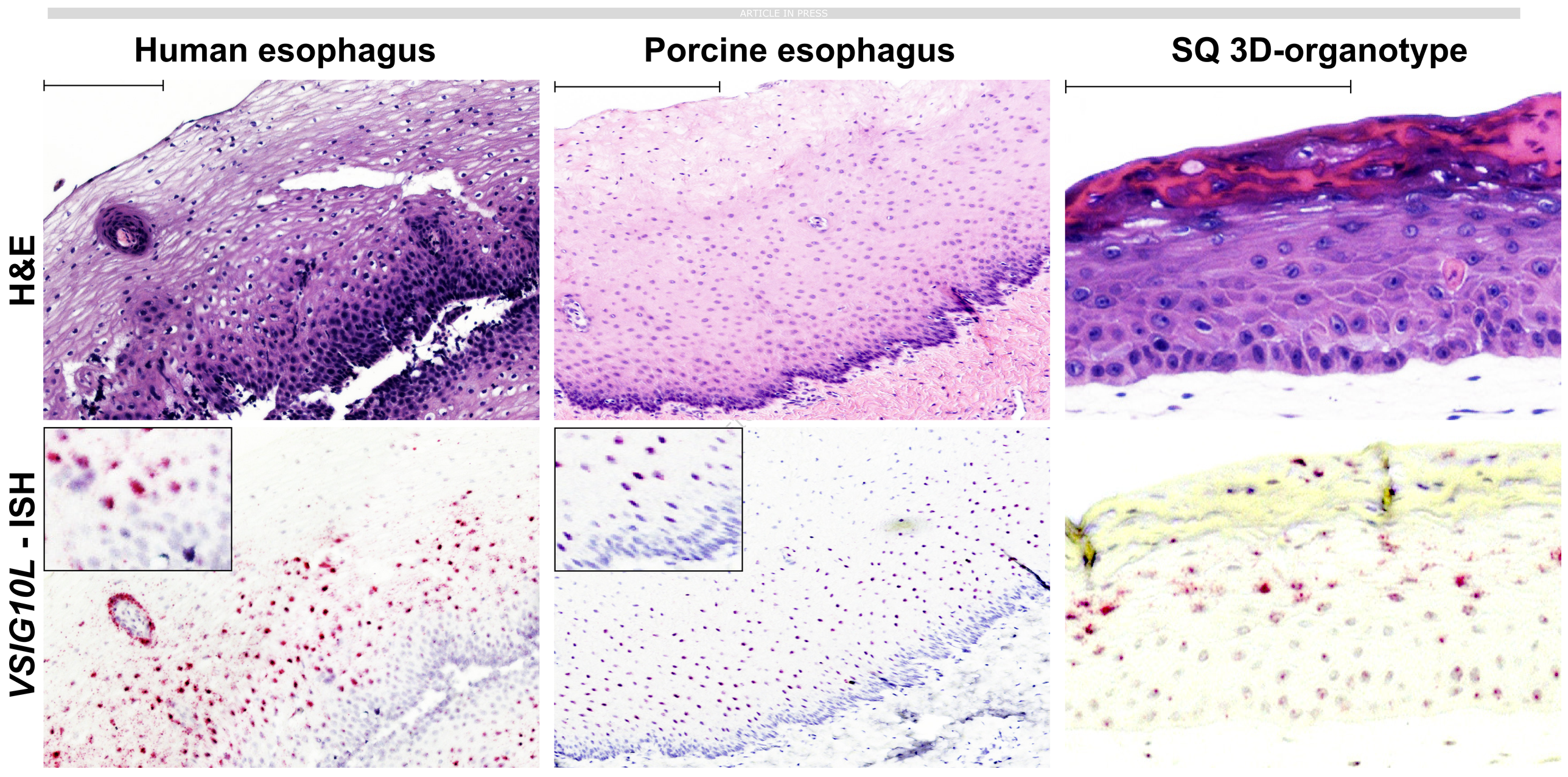
Human esophagus
Porcine esophagus
SQ 3D-organotype
H&E
VSIG10L - ISH

Control subject

H&E

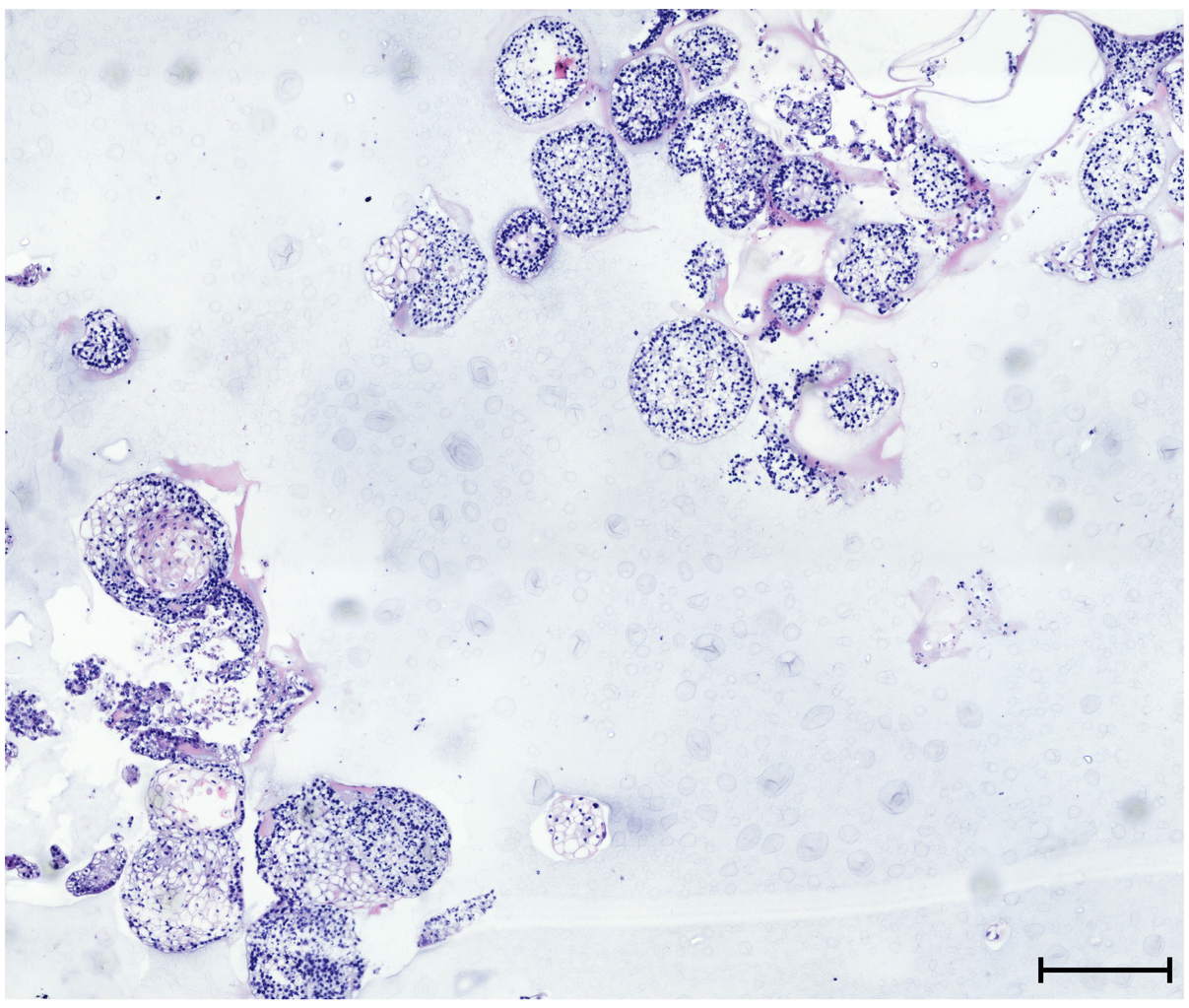

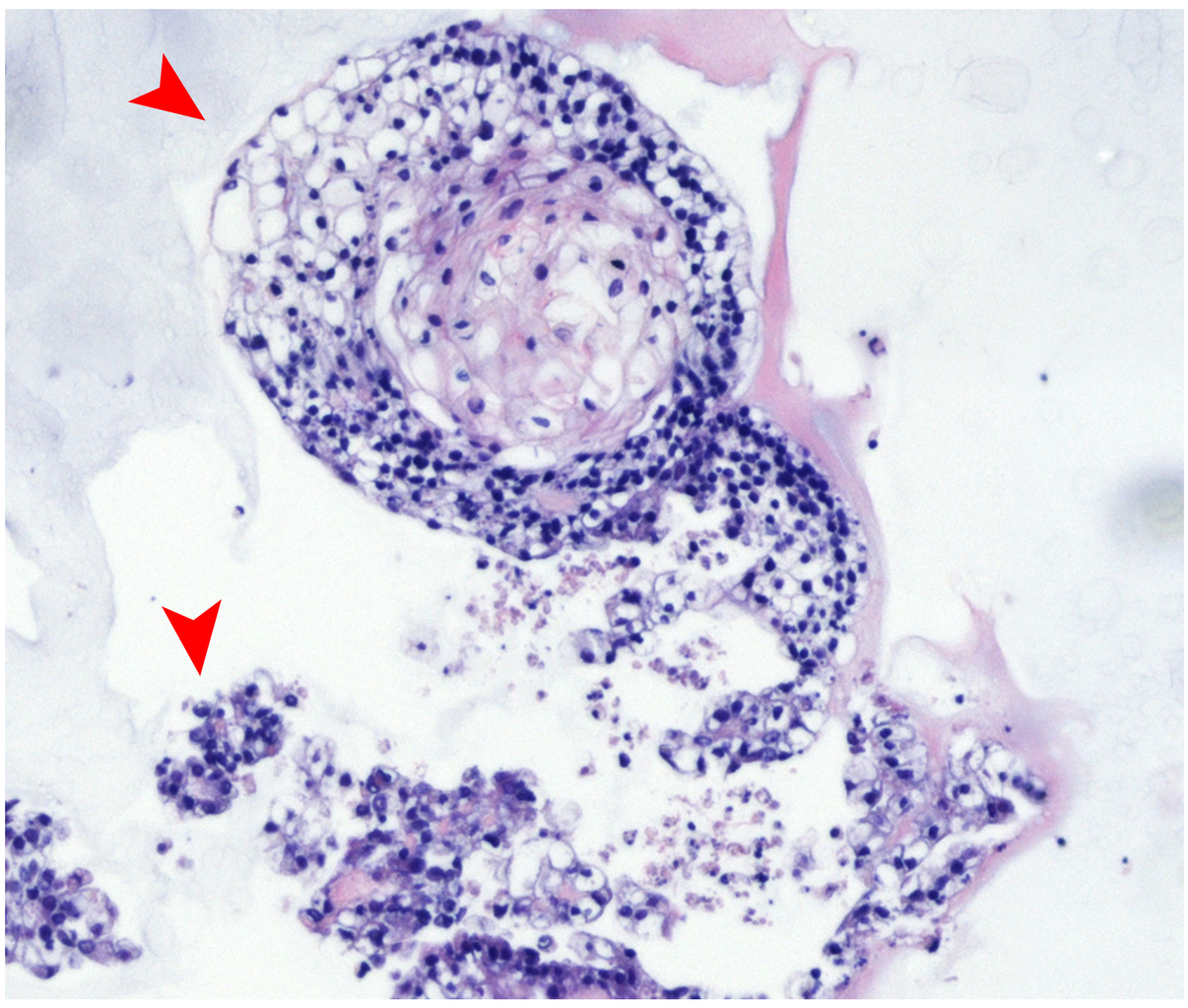

p63

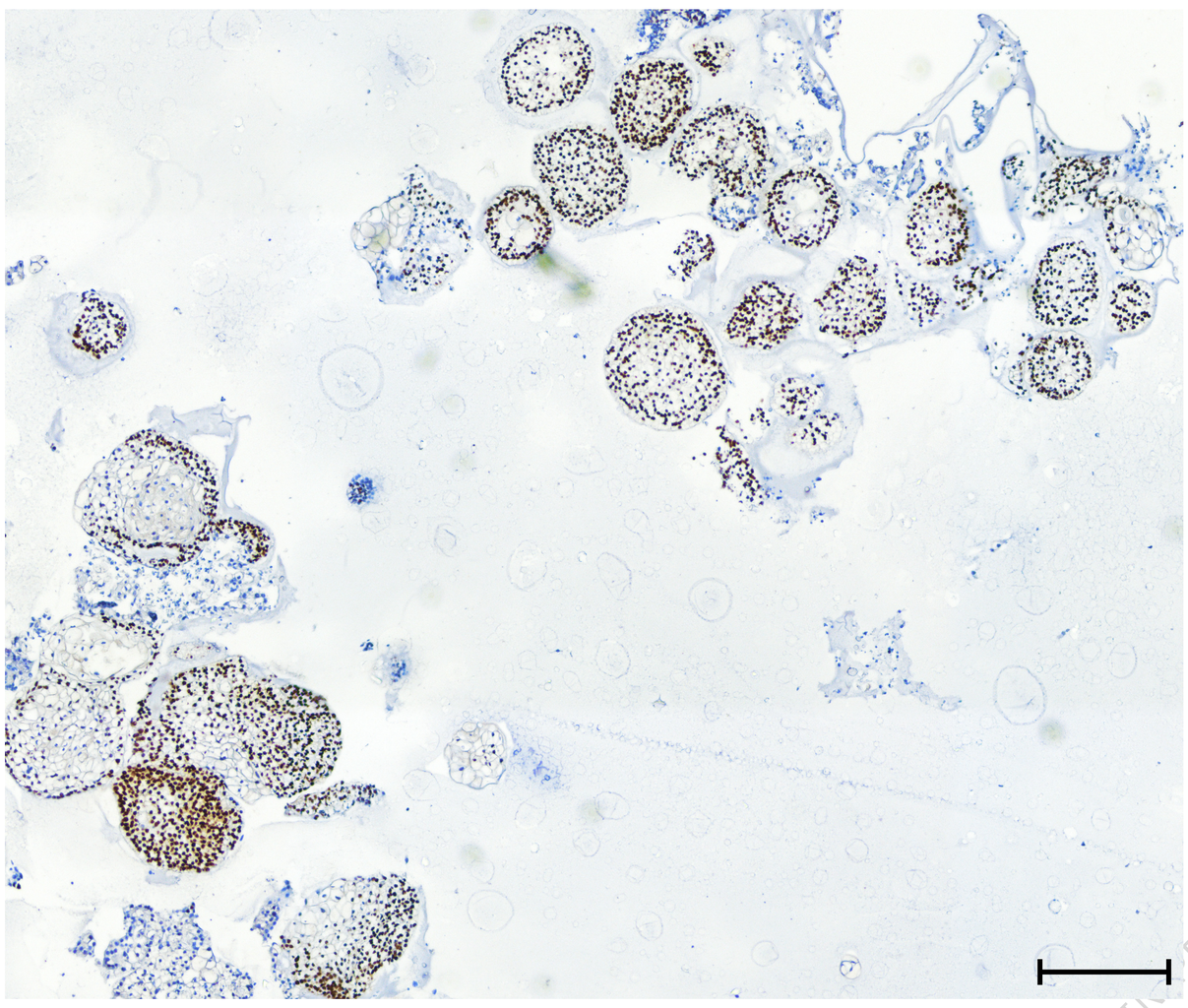

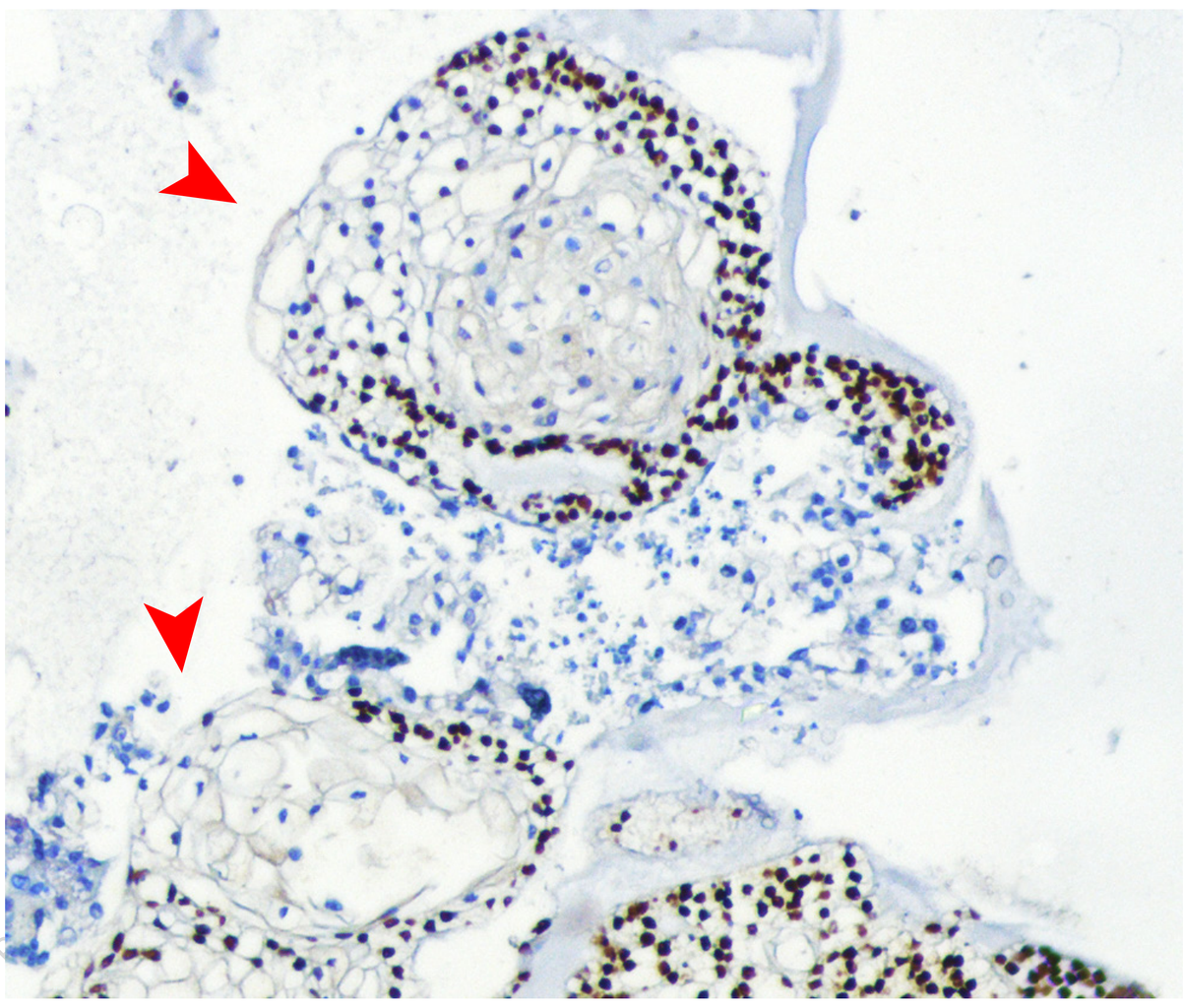

VSIG10L S631G-mutant patient

H&E

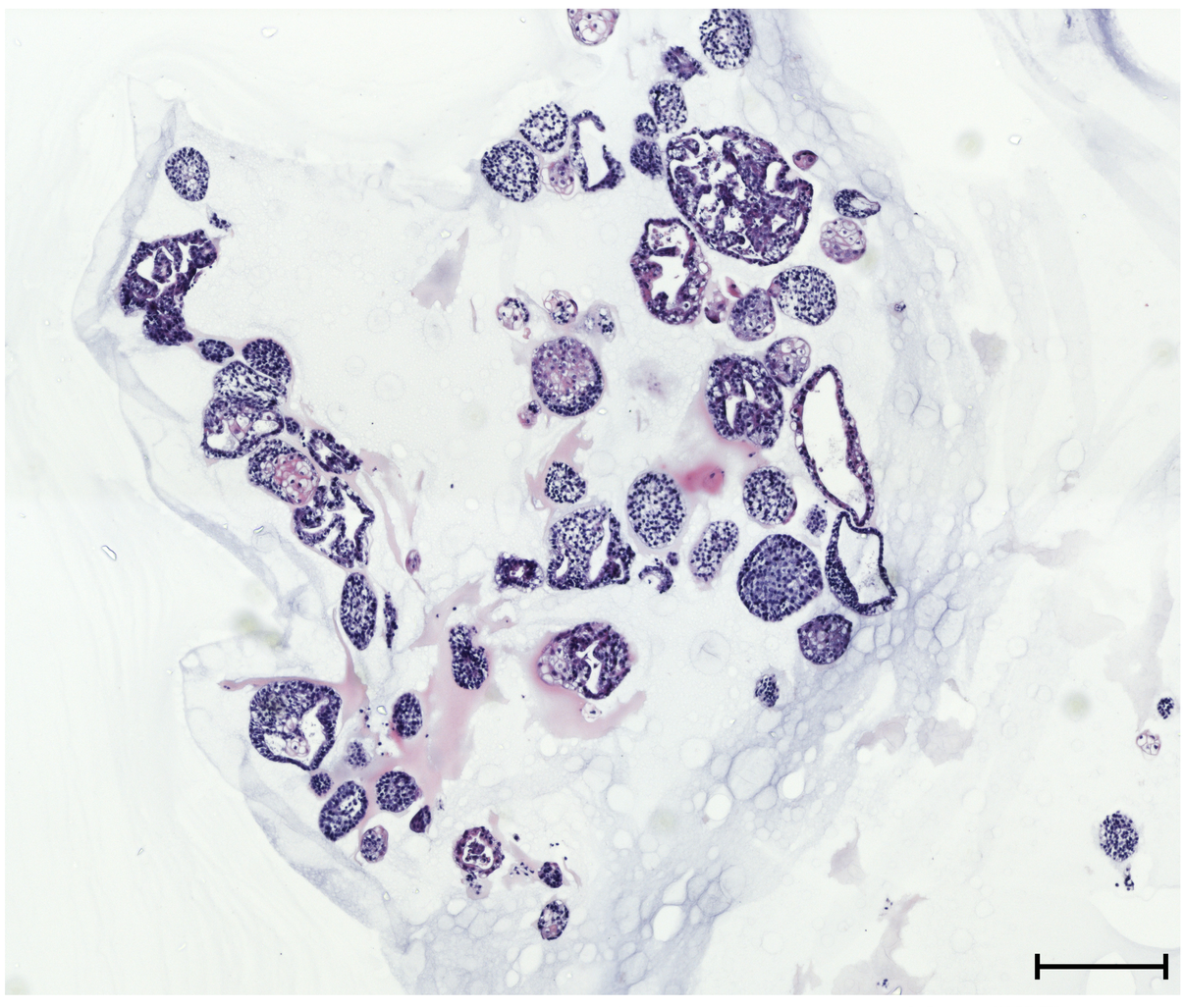

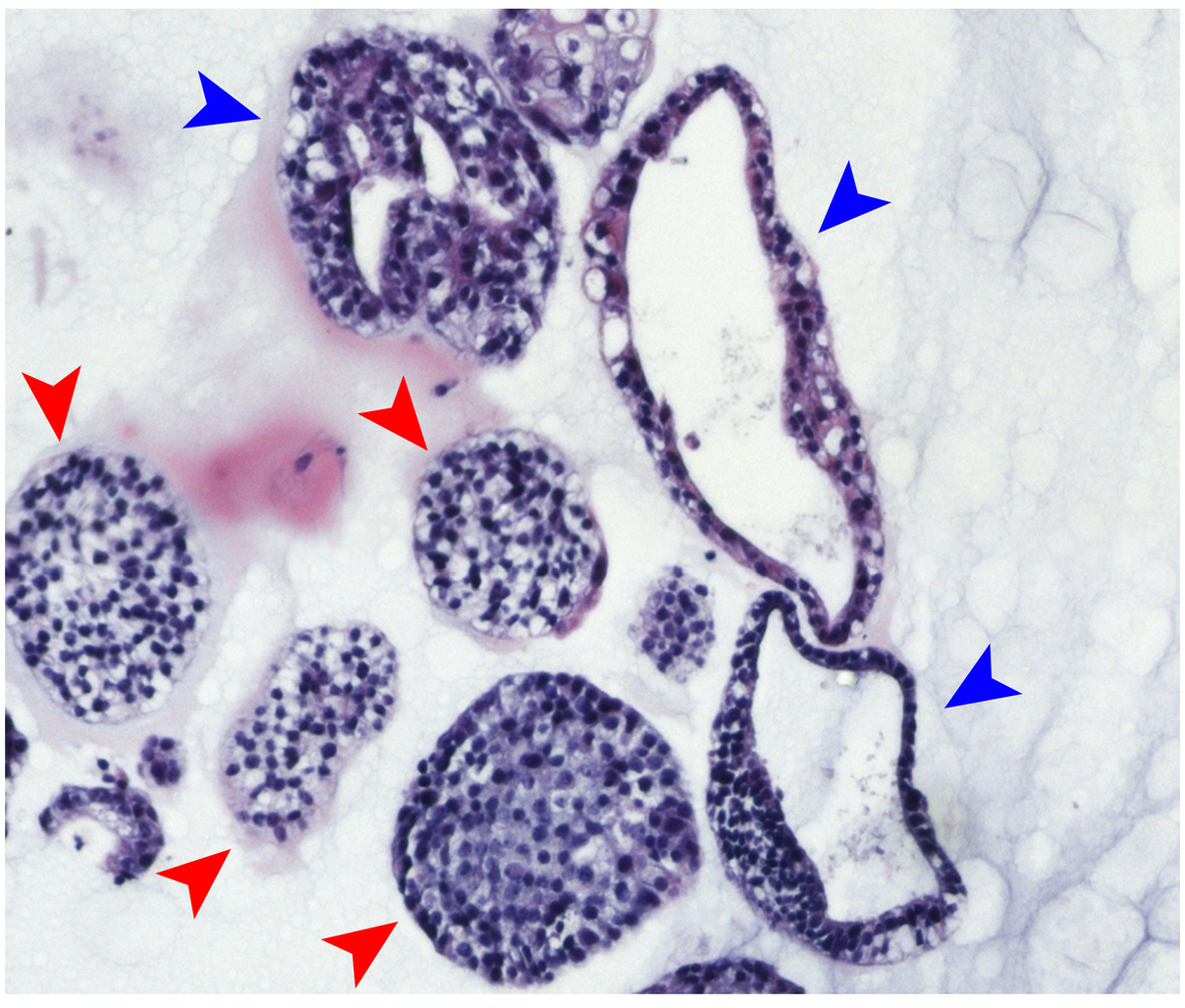

p63

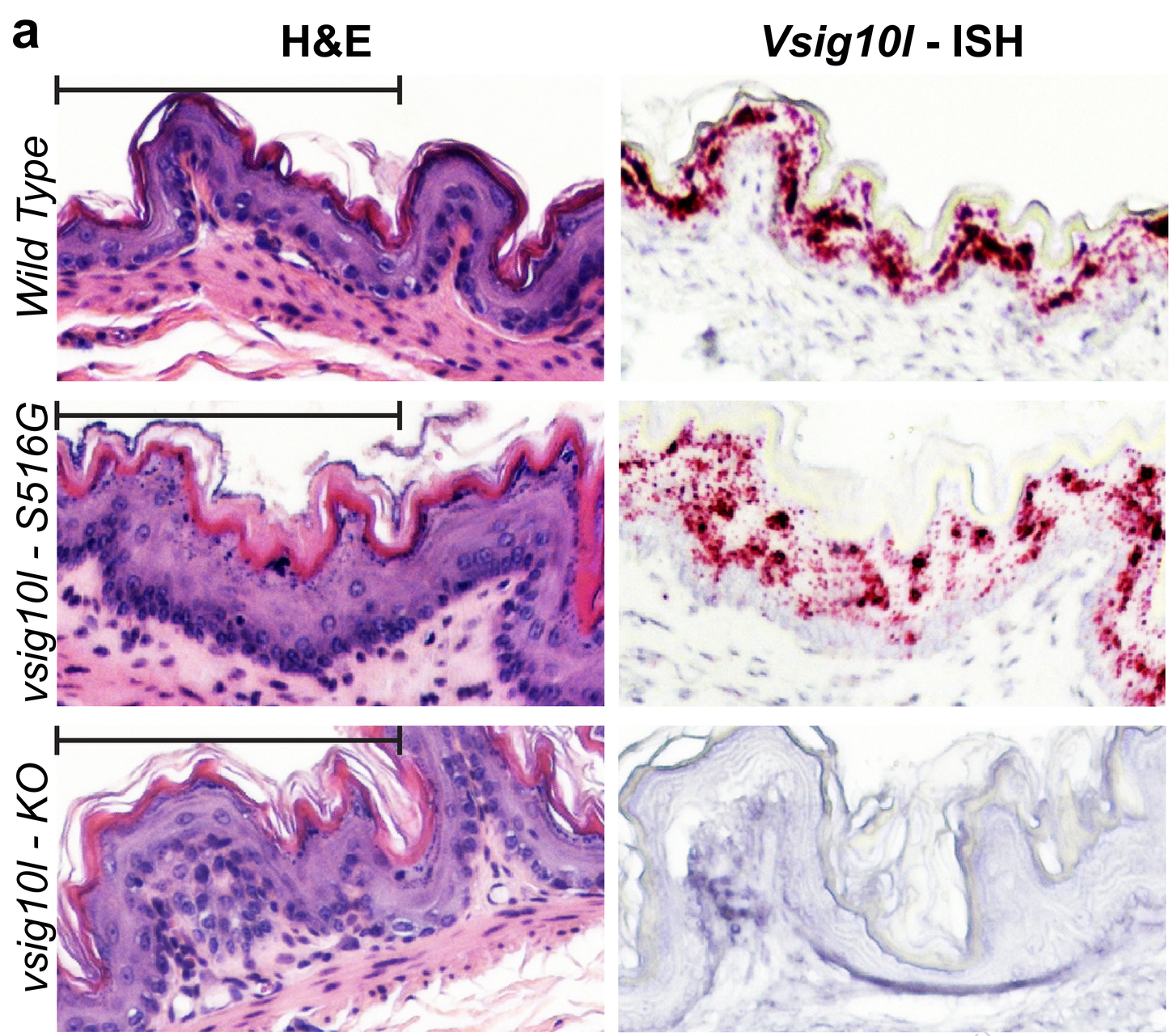

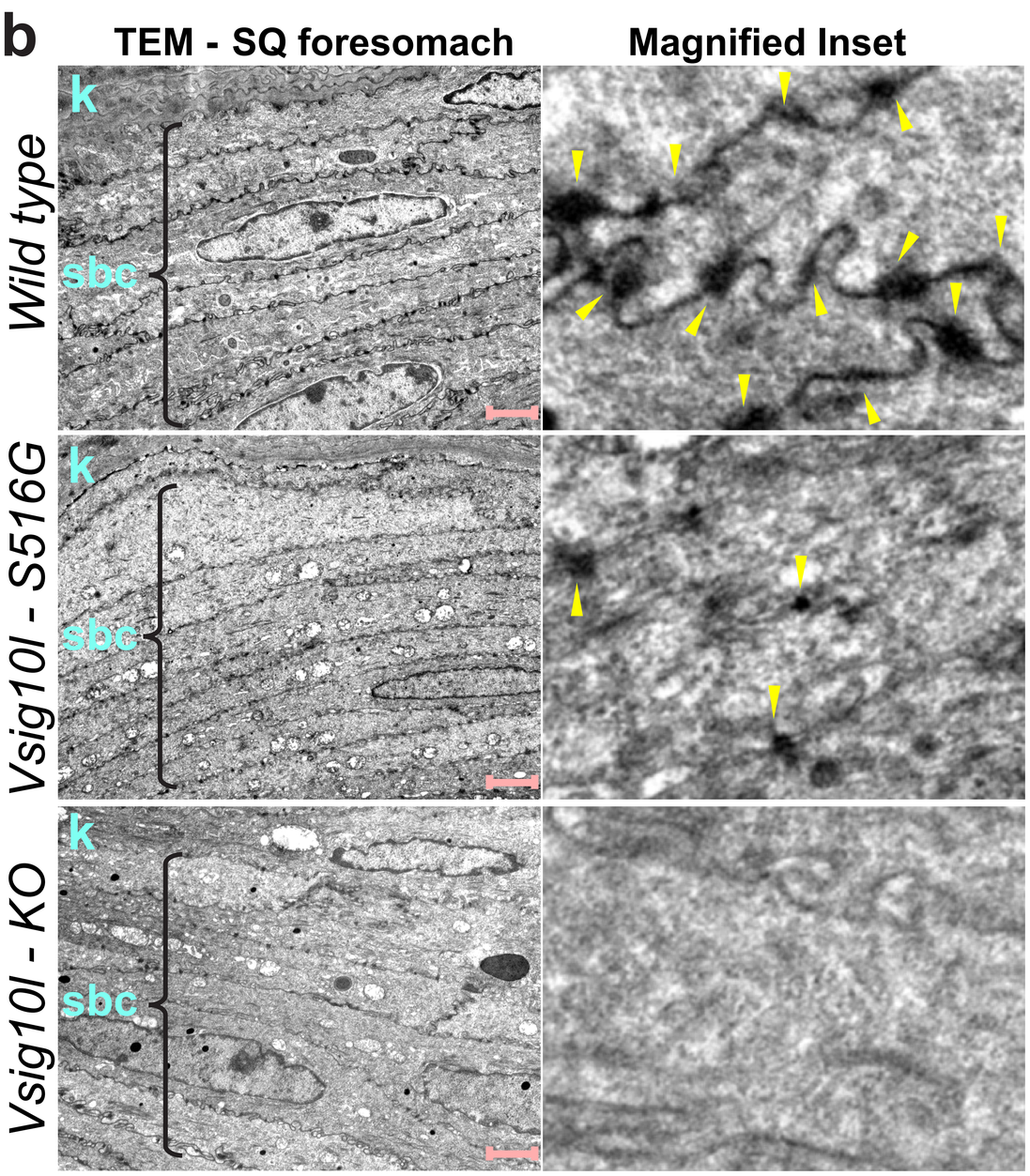

k (Keratinized layer); **sbc** (superficial/suprabasal cells)

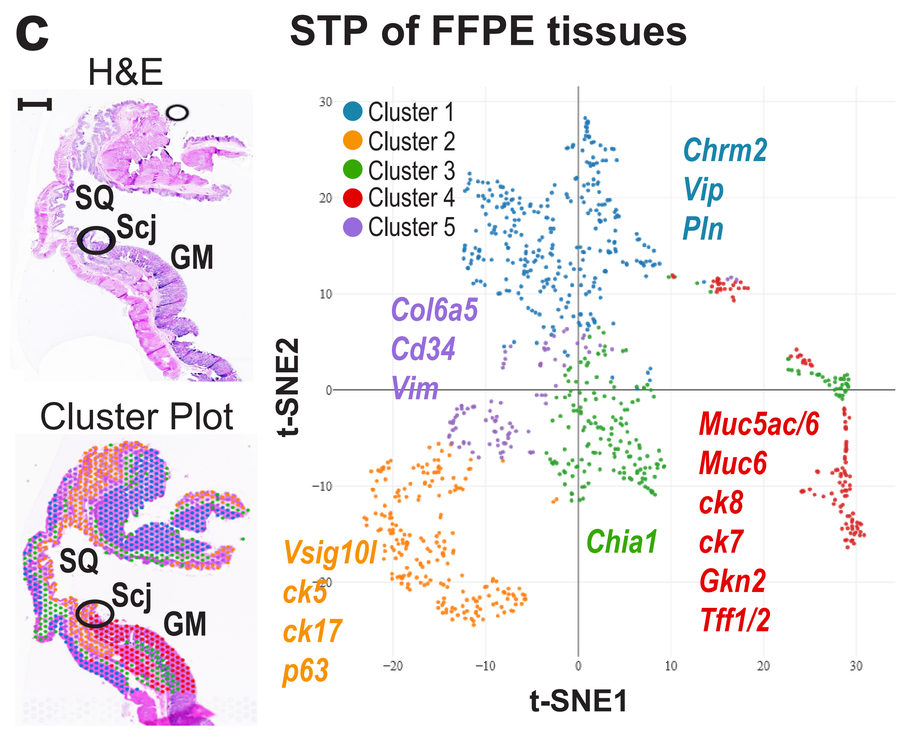

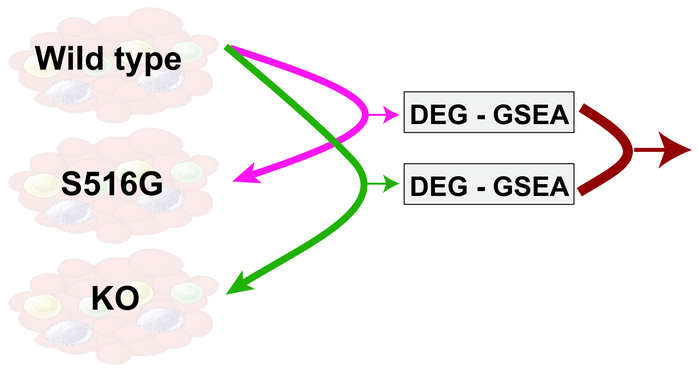

Gene Ontology (GO)	Adj P-value
GO:CC; CORNIFIED ENVELOPE	*P = 5.039E-06*
GO:BP; EPIDERMAL CELL DIFFERENTIATION	*P = 0.014*
GO:MF; STRUCTURAL MOLECULE ACTIVITY	*P = 0.007*

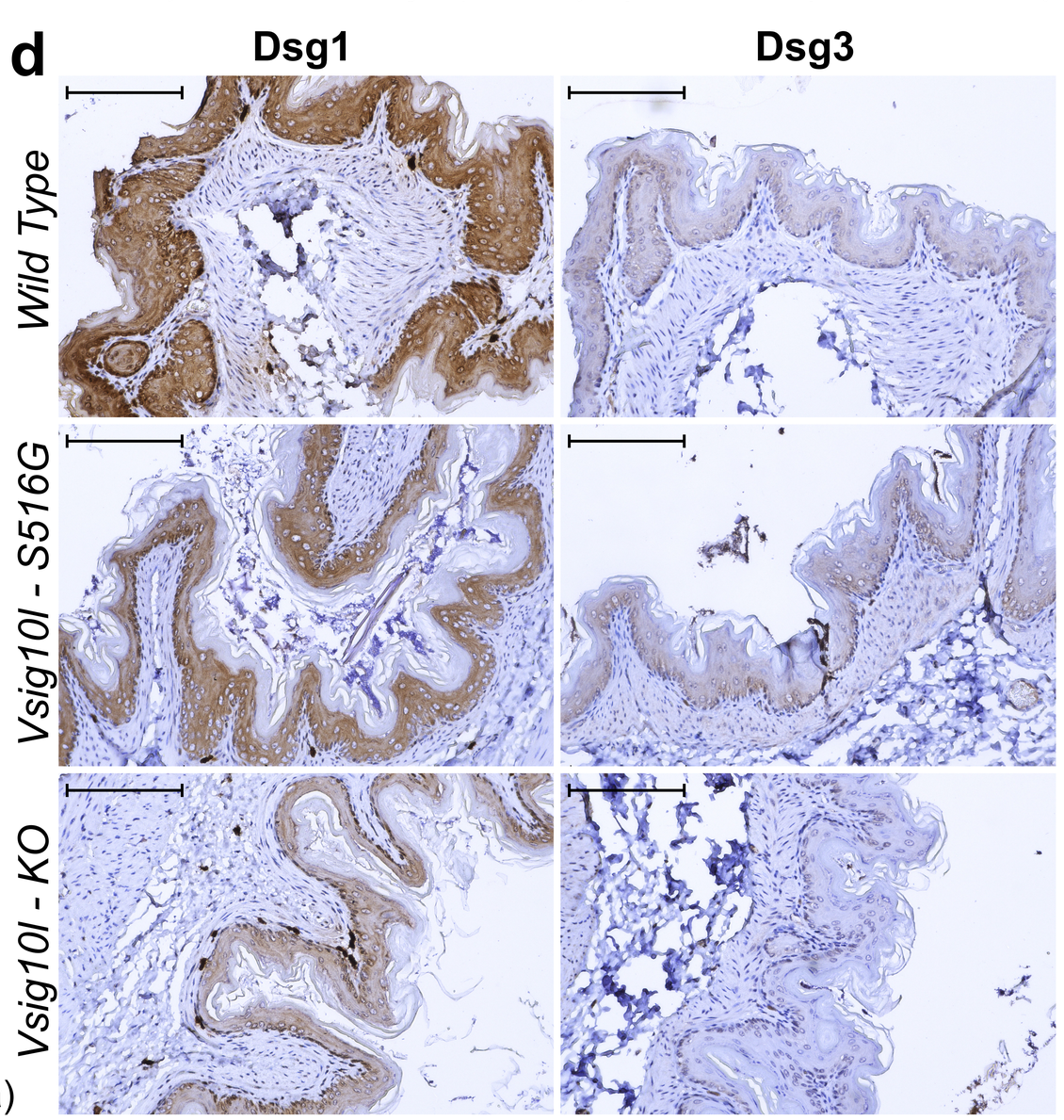

SQ (squamous epithelia); **Scj** (squamo-columnar junction); **GM** (gastric mucosa)

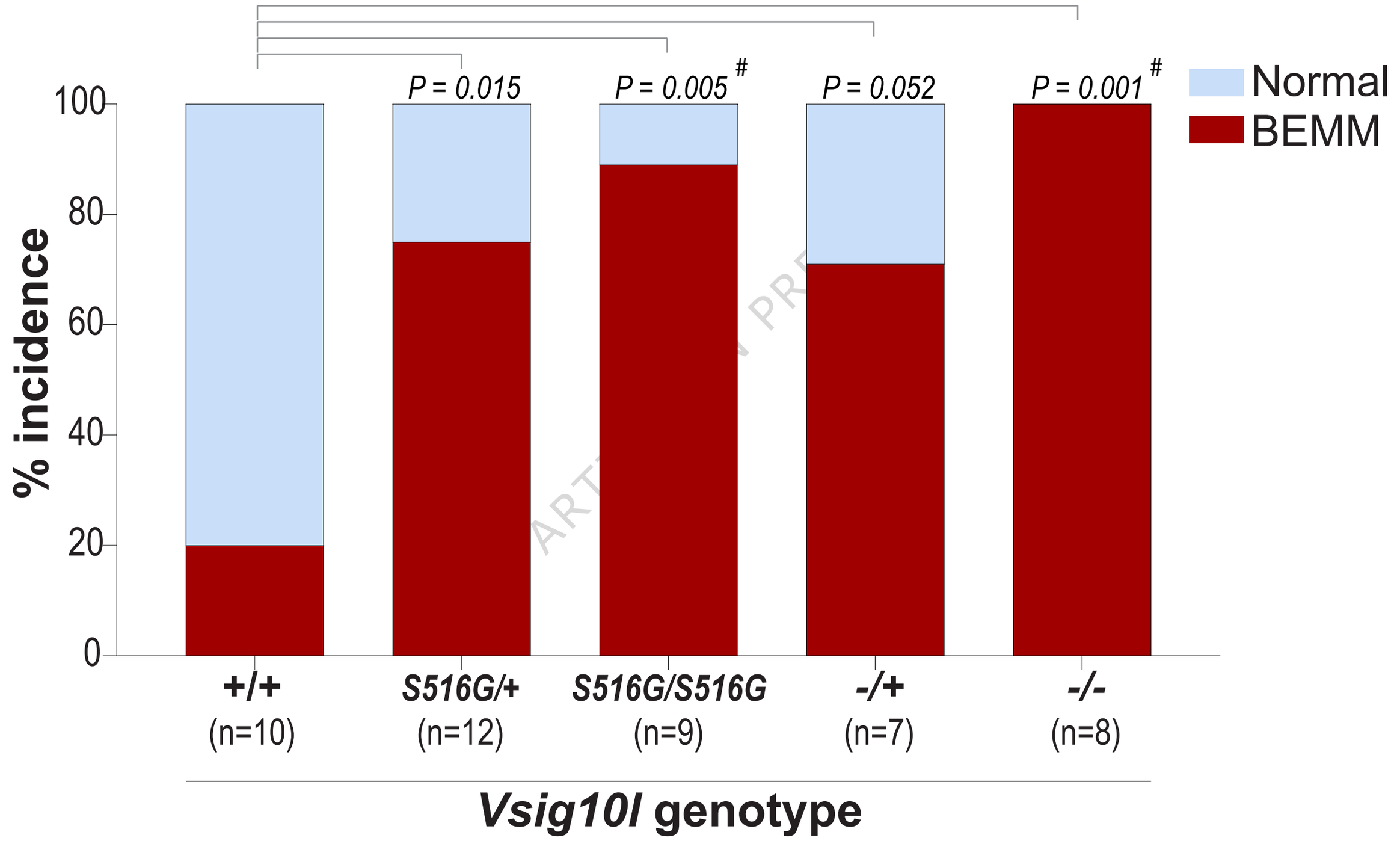
P = 0.015
P = 0.005 #
P = 0.052
P = 0.001 #
Normal
BEMM
100
80
60
40
20
0
% incidence
+/+
(n=10)
S516G/+
(n=12)
S516G/S516G
(n=9)
-/+
(n=7)
-/-
(n=8)
Vsig10l genotype

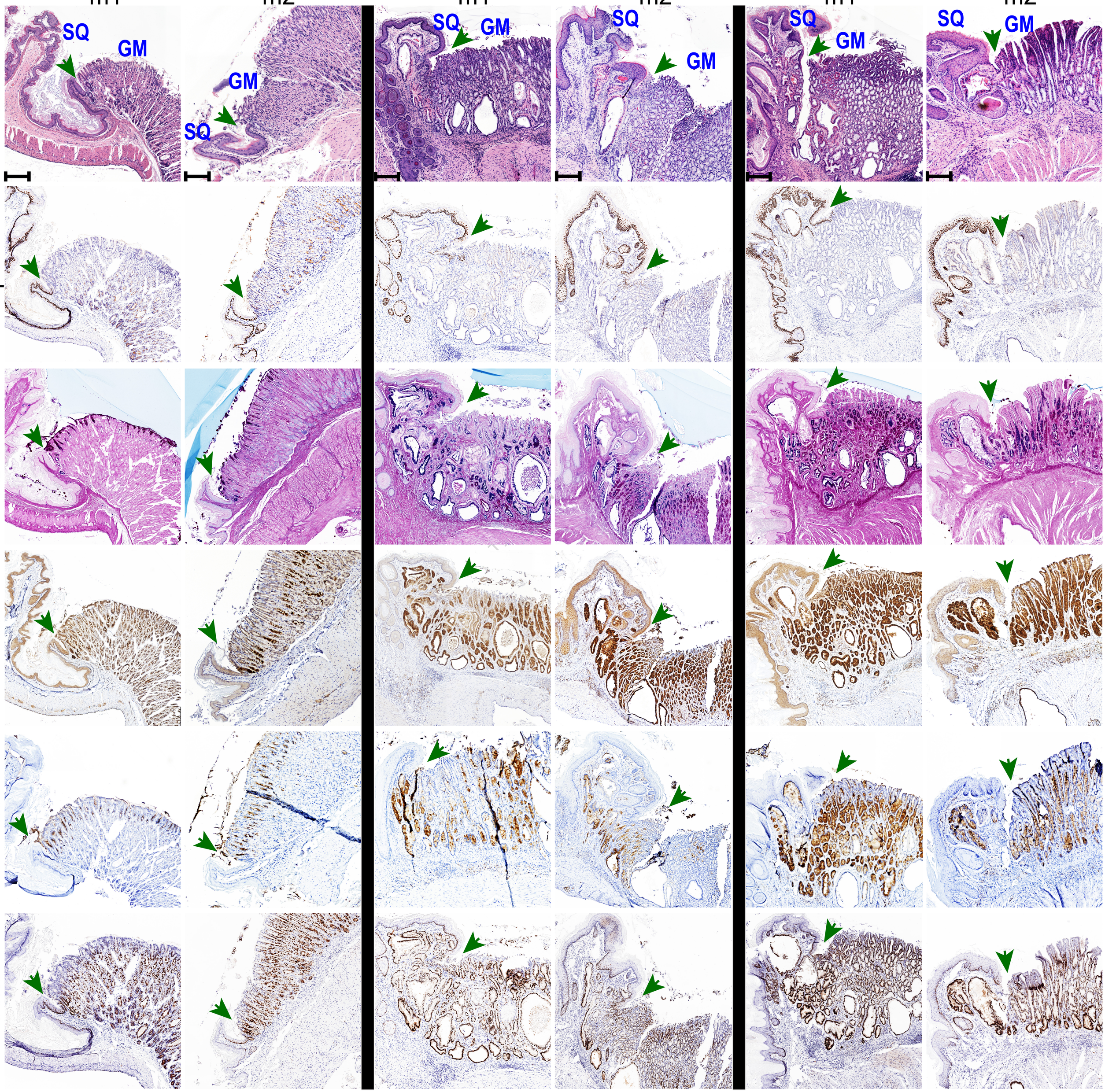
Wild type
Vsig10l - S516G
Vsig10l - KO
m1
m2
m1
m2
m1
m2
H&E
p63
AB-PAS
Muc6
Tff3
Sox9
SQ
GM

a

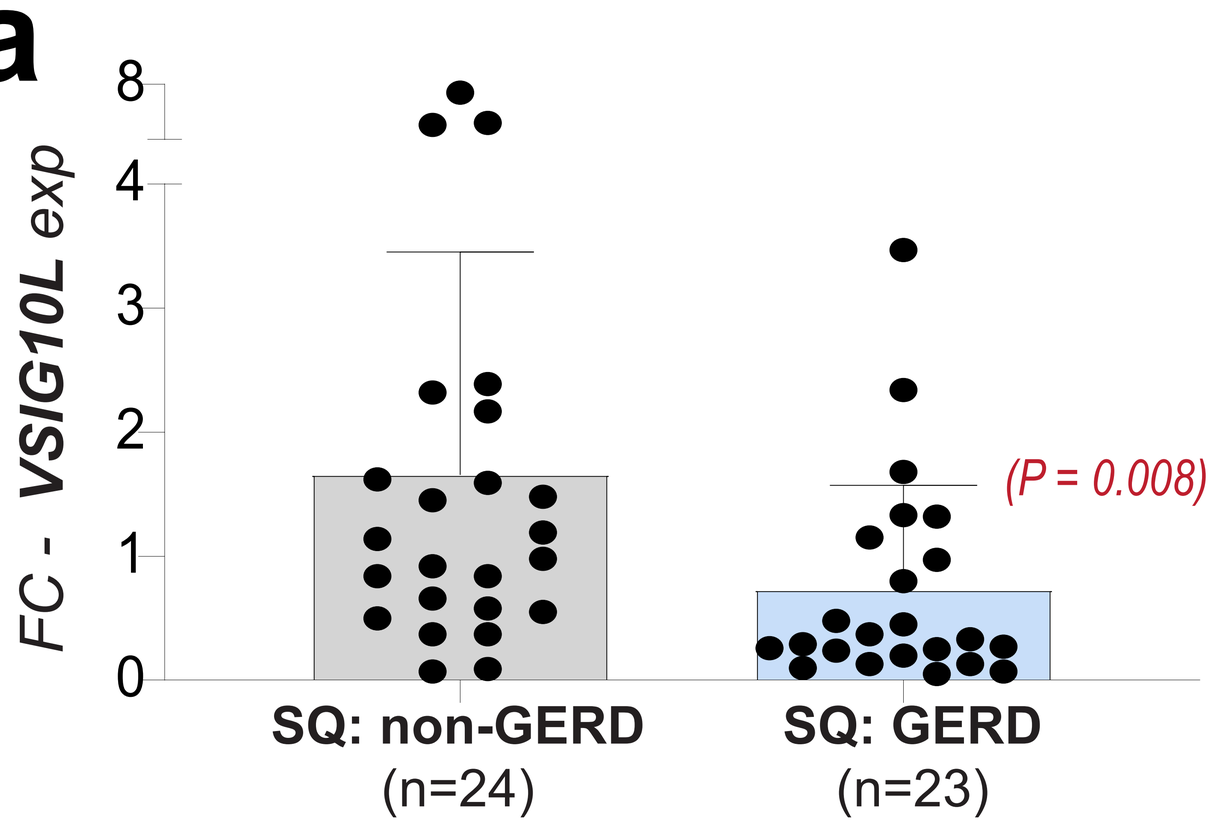
FC - VSIG10L exp
8
4
3
2
1
0
(P = 0.008)
SQ: non-GERD
(n=24)
SQ: GERD
(n=23)

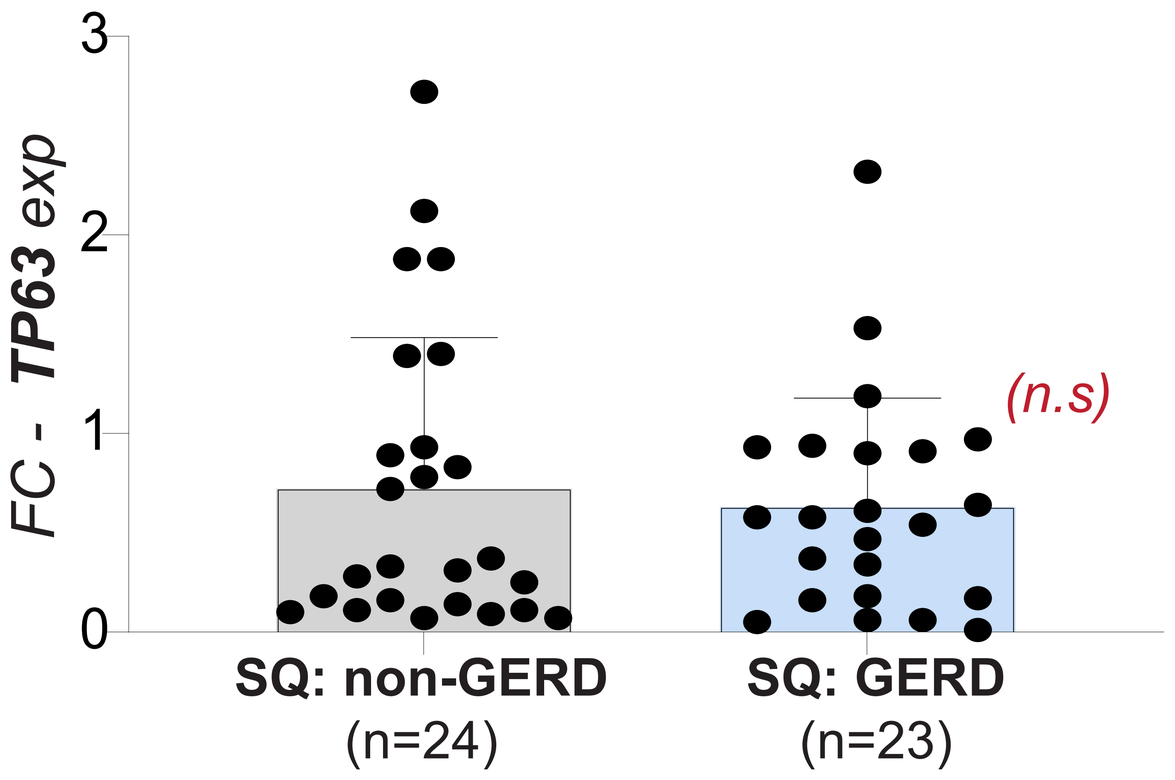
FC - TP63 exp
3
2
1
0
(n.s)
SQ: non-GERD
(n=24)
SQ: GERD
(n=23)

b

H&E
p63 - IHC
VSIG10L - ISH
Healthy esophageal SQ mucosa
GERD - P1
GERD - P2
GERD - P3
GERD - P4
GERD - P5